Supporting information:

Dimethyl Sulfoxide Complexes Detected at Ambient Conditions

Anne S. Hansen and Henrik G. Kjaergaard*

Department of Chemistry, University of Copenhagen, Universitetsparken 5, DK-2100 Copenhagen, Denmark

E-mail: hgk@chem.ku.dk

Phone: +45-35320334. Fax: +45-35320322

*To whom correspondence should be addressed

Contents

S1 Experimental

S1.1 Band integration and fitting

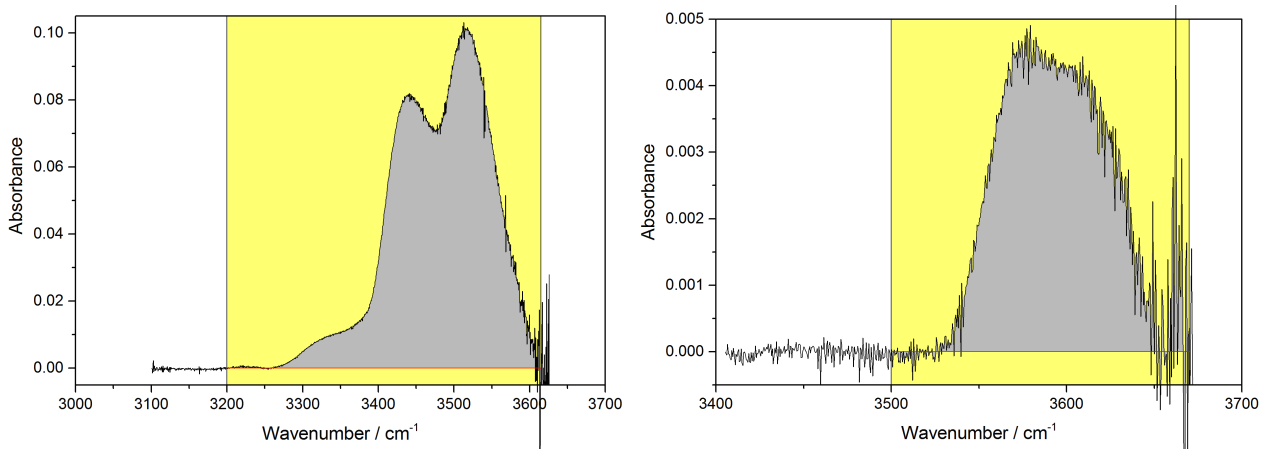

(a) (b)

Figure S1: Band integration of the OH-stretching transition in the MeOH·DMSO (a) and MeOH·acetone (b) complexes. The integration ranges are 3200 - 3615 cm^{-1} and 3500 - 3670 cm^{-1} in (a) and (b), respectively.

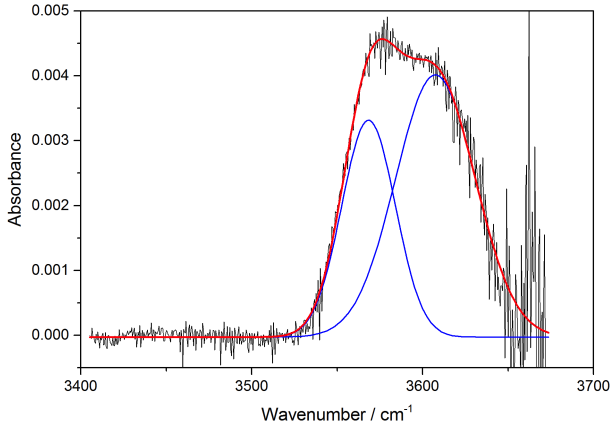

Figure S2: Gaussian functions fitted to the OH-stretching band in the MeOH·acetone complex.

S1.2 Matrix spectra

In Figure S3, we show the 12 K Ar matrix spectra of the monomers and the mixtures: water + DMSO, MeOH + DMSO, water + acetone, and MeOH + acetone. Slightly different amounts of water vapor (∼1 Torr) were used in the water + DMSO and water + acetone mixtures. Consequently the water monomer spectra presented in Figure S3 are recorded at slightly different pressures. The bands observed in the 3310 - 3410 cm^{-1} region are assigned to the OH-stretching vibration in the H_2O·DMSO and MeOH·DMSO complexes, which is redshifted relative to the transition observed for water[1] and MeOH.[2–4] Likewise, the bands observed in the 3480 - 3530 cm^{-1} region of the water + acetone and MeOH + acetone spectra are assigned to the OH-stretching vibration in the H_2O·acetone and MeOH·acetone complexes. In addition to the spectra recorded at 12 K, annealing experiments were performed. Upon annealing, the band intensity of the OH-stretching vibration in the complexes increases, which indicates that more complex is formed. In the 3340 - 3390 cm^{-1} region peaks are observed in the 12 K Ar matrix spectra of DMSO (∼3362 cm^{-1} and ∼3383 cm^{-1}) and MeOH, which are close to, but different from those observed in the water + DMSO and MeOH + DMSO mixtures. These weak features have previously been observed and assigned to combination bands of DMSO.[5] In the spectrum of MeOH, absorbance is observed in the ∼3500 - 3560 cm^{-1} region. The peaks arise from the OH-stretching vibration of MeOH clusters,[6–9] which, unfortunately, overlap with those in the spectrum of the MeOH + acetone mixture. Water clusters can also form; however, the OH-stretching transition from the water dimer is outside of our region of interest, 3574 - 3633 cm^{-1} and 3708 - 3738 cm^{-1}.[1] The higher order water complexes (mainly trimer) are observed in the ∼3200 - 3550 cm^{-1} region.[1] These transitions are insignificant due to the low water pressure used. The spectra of the water + acetone and MeOH + acetone mixtures are in agreement with previous Ar matrix measurements,[10,11] besides the peak at 3510 cm^{-1} in the spectrum of the water + acetone mixture, which was not previously reported. For the MeOH·acetone complex the peaks observed at 3518 cm^{-1} and 3503 cm^{-1} have been assigned to different MeOH·acetone

conformers based on a theoretical investigation.[11]

For the complexes with acetone as the hydrogen bond acceptor, the CO-stretching vibration was also observed. The CO-stretching vibration in the H_2O·acetone and MeOH·acetone complexes is redshifted relative to that in the acetone monomer. The shift is ∼5 cm^{-1} in agreement with previous observations.[10,11] The SO-stretching vibration of DMSO was not observed, as it lies outside our detection range, caused by the matrix CaF_2 window.

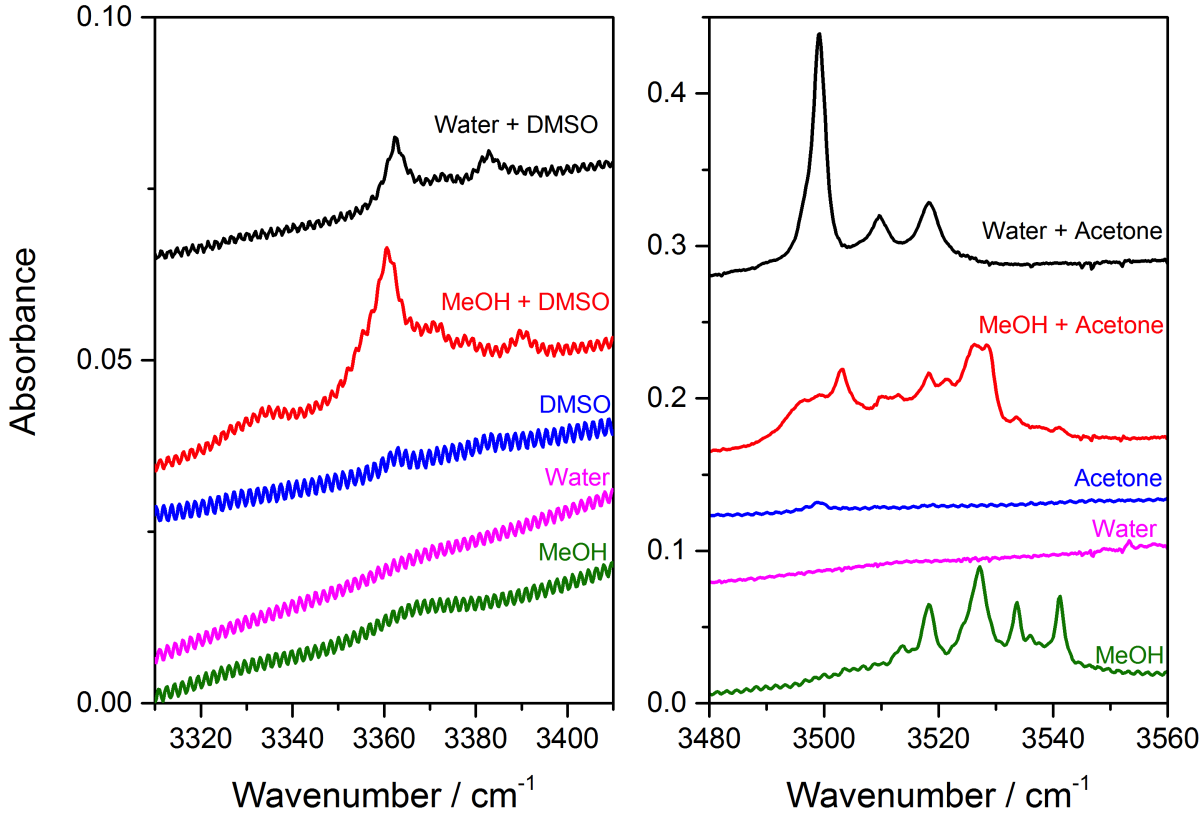

Figure S3: 12 K Ar matrix FTIR spectra of DMSO (left, 3310 - 3410 cm^{-1} region) and acetone (right, 3480 - 3560 cm^{-1} region) monomers and spectra of their mixtures with water (black) and MeOH (red). For the left side of the figure the mixing ratios are: H_2O/DMSO/Ar 1:1:715 Torr; MeOH/DMSO/Ar 1:1:718 Torr; DMSO/Ar 1:678 Torr; H_2O/Ar 1:716 Torr; MeOH/Ar 1:716 Torr. For the right side: H_2O/acetone/Ar 2:1:718 Torr; MeOH/acetone/Ar 1:1:710 Torr; acetone/Ar 1:710 Torr; H_2O/Ar 2:718 Torr; MeOH/Ar 1:716 Torr.

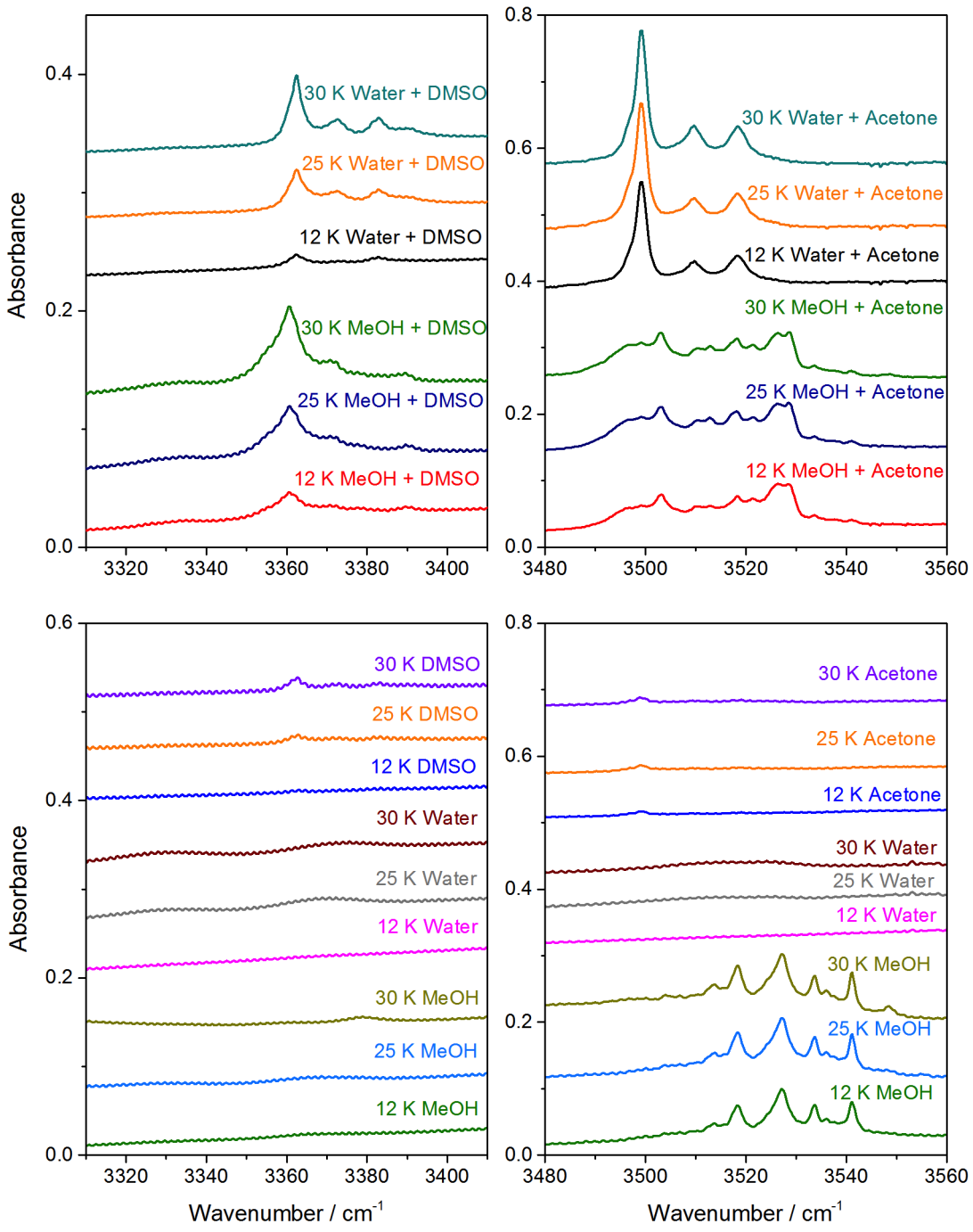

Figure S4: Ar Matrix FTIR spectra of H_2O + acetone and MeOH + acetone mixtures, and the corresponding monomers recorded after annealing at 12 K, 25 K and 30 K. The mixing ratios correspond to those given in Figure S3.

The CO-stretching region:

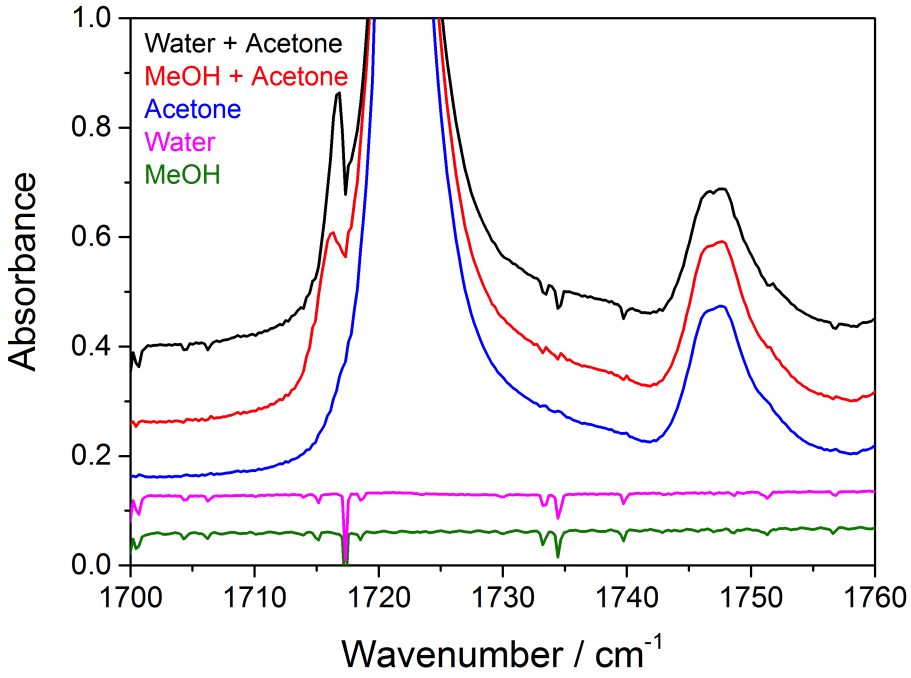

Figure S5: Ar Matrix FTIR spectra of H_2O + acetone and MeOH + acetone mixtures, and the corresponding monomers in the CO-stretching region.

OH-stretching vibrations in water:

The water monomer has 3 vibrational modes: a symmetric OH-stretching vibration (ν_1), an asymmetric OH-stretching vibration (ν_3) and a HOH-bending motion (ν_2). The water dimer has 12 vibrational modes, and the two water units in the dimer are referred to as the proton donor (PD) and proton acceptor (PA), respectively. Ar matrix spectra of water have previously been recorded, and in Table S1 we summarize the work by Perchard.[1] For the proton donor we label the vibrational modes as $|x\rangle_{\mathrm{f}}\,|y\rangle_{\mathrm{b}}\,|z\rangle$, where x is the number of vibrational quanta in the OH_f stretching mode, y the quanta in the OH_b stretching mode and z the quanta in the H_fOH_b bending mode. For the proton acceptor the vibrational modes are given by the $|xy\rangle_{\pm}\,|z\rangle$ notation for the equivalent modes. The $\pm$ refers to the symmetric and asymmetric stretching vibrations.

In the 3711 - 3776 cm^{-1} region the asymmetric OH-stretching vibration (ν_3) of the

water monomer is observed.[1] Upon complexation this vibration is redshifted and observed in the 3708 - 3738 cm^{-1} region. The bands observed arise from both the proton acceptor (PA) and proton donor (PD). The symmetric OH-stretching vibration (ν_1) of the water monomer is observed in the 3607 - 3670 cm^{-1} region. The ν_1 vibration is also redshifted upon complexation and is observed at 3574 and 3633 cm^{-1} for the PD and PA units, respectively. At lower frequencies (e.g. 3210 - 3528 cm^{-1}) higher order complexes are reported, which mainly arise from clusters consisting of three H_2O molecules.

Table S1: Observed frequencies (cm^{-1}) in the Ar matix spectra of water.

	Previous study at 10 K[a]	
Mode	Band	$\tilde{\nu}$
$\|10\rangle_- \|0\rangle$	ν_3 (PA)	3738, 3716
$\|1\rangle_f \|0\rangle_b \|0\rangle$	ν_3 (PD)	3708
$\|10\rangle_+ \|0\rangle$	ν_1 (PA)	3633
$\|0\rangle_f \|1\rangle_b \|0\rangle$	ν_1 (PD)	3574
-	ν_{OH_b} HO (T)	3528, 3516, 3380, 3330, 3210
-	ν_{OH_f} HO (T)	3700, 3695

Acronyms: PA: proton acceptor, PD: proton donor, HO: higher order, T: trimer.
a: ref.[1]

S1.3 Vibrational gas phase spectra of monomers

In Figures S6 - S7, Figures S8 - S10 and Figure S11 - S13, we show spectra of the MeOH, DMSO and acetone monomers, respectively. The MeOH and DMSO spectra were recorded with a 16 m cell and the acetone spectrum with a 20 cm cell. The combination of the optical path length and the monomer pressure used causes saturation of some transitions. However, the saturated transitions lie outside our region of interest, the OH-stretching region, and do not effect our spectral subtraction. Prior to these monomer spectra, we recorded spectra of their mixtures (MeOH + DMSO and/or MeOH + acetone). The cell was left to pump on a vacuum line for 1 hour before recording the monomer spectra. However, MeOH is sticky and difficult to pump out, and in the spectra of DMSO and acetone small MeOH leftovers may be present.

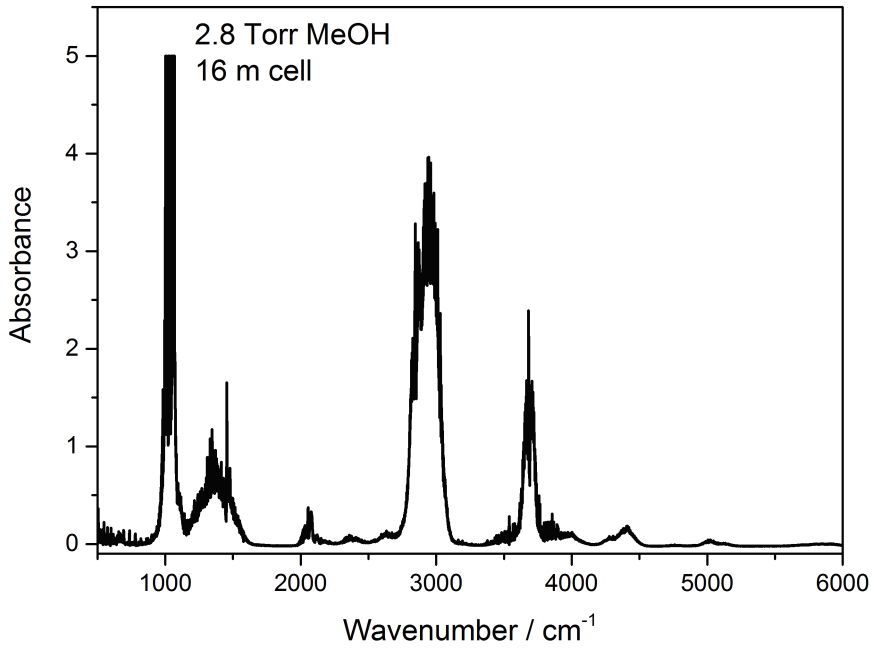

Figure S6: Spectrum of gas phase MeOH monomer in the 500 - 6000 cm^{-1} region.

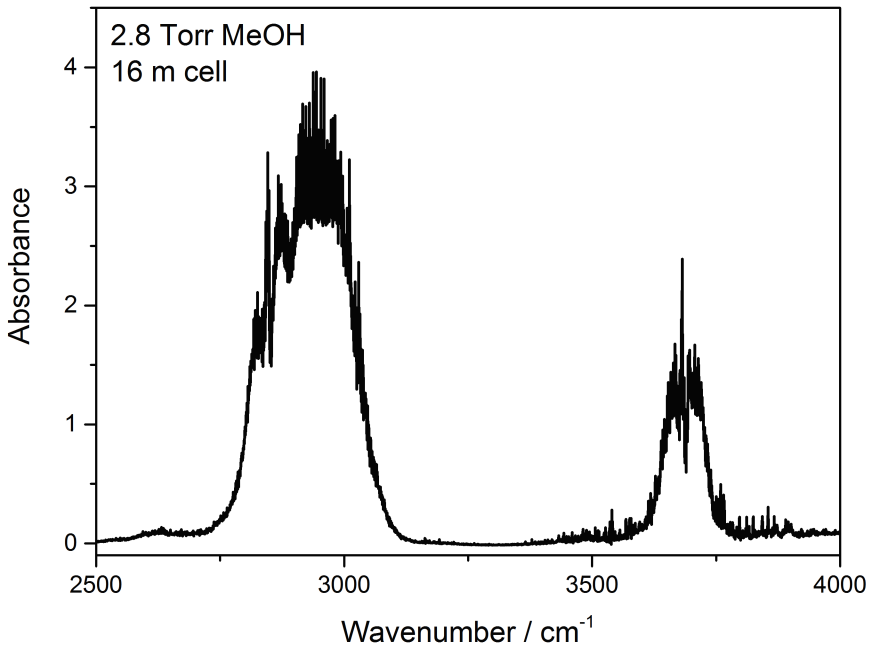

Figure S7: Spectrum of gas phase MeOH monomer in the 2500 - 4000 cm^{-1} region.

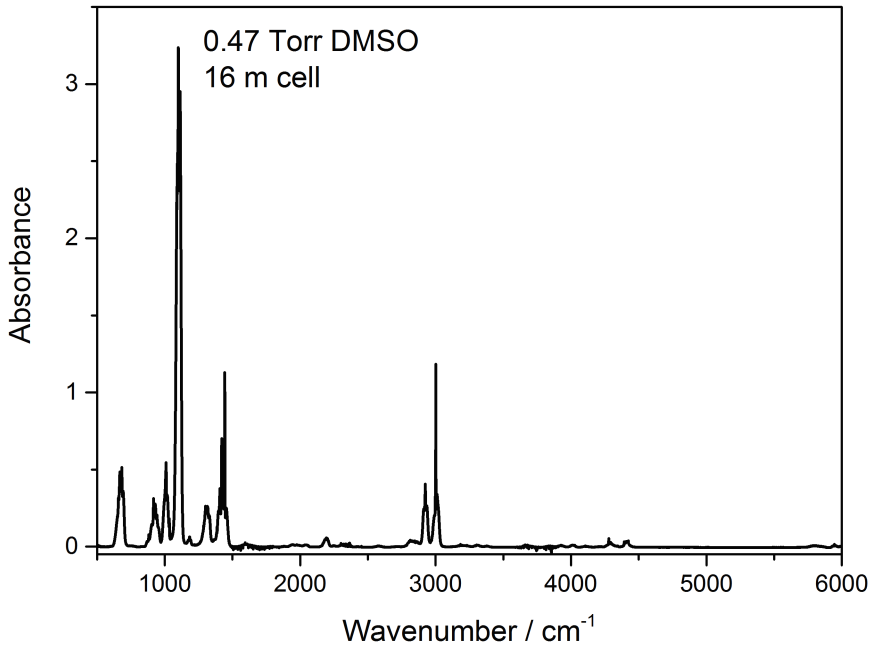

Figure S8: Spectrum of gas phase DMSO monomer in the 500 - 6000 cm^{-1} region.

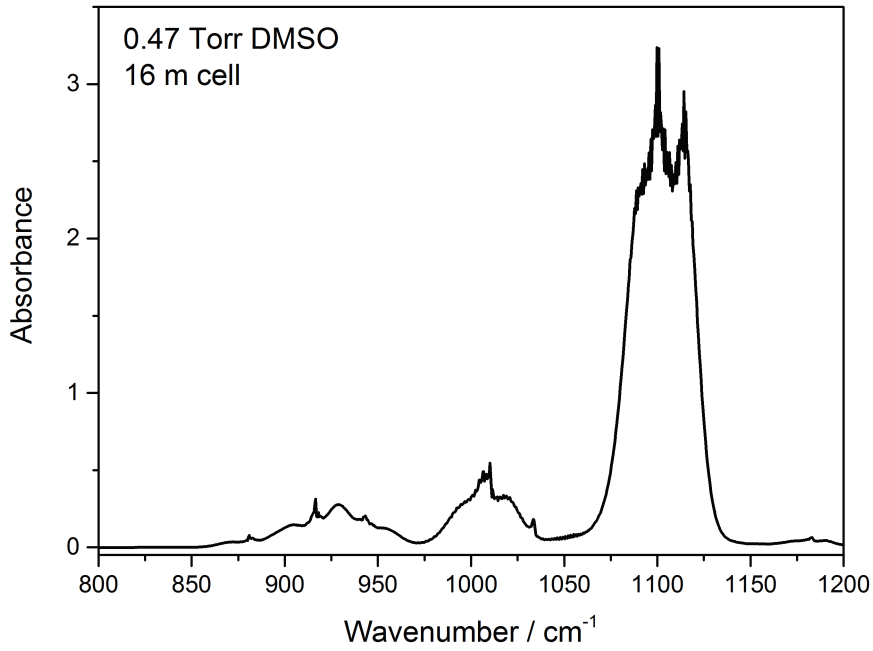

Figure S9: Spectrum of gas phase DMSO monomer in the 800 - 1200 cm^{-1} region.

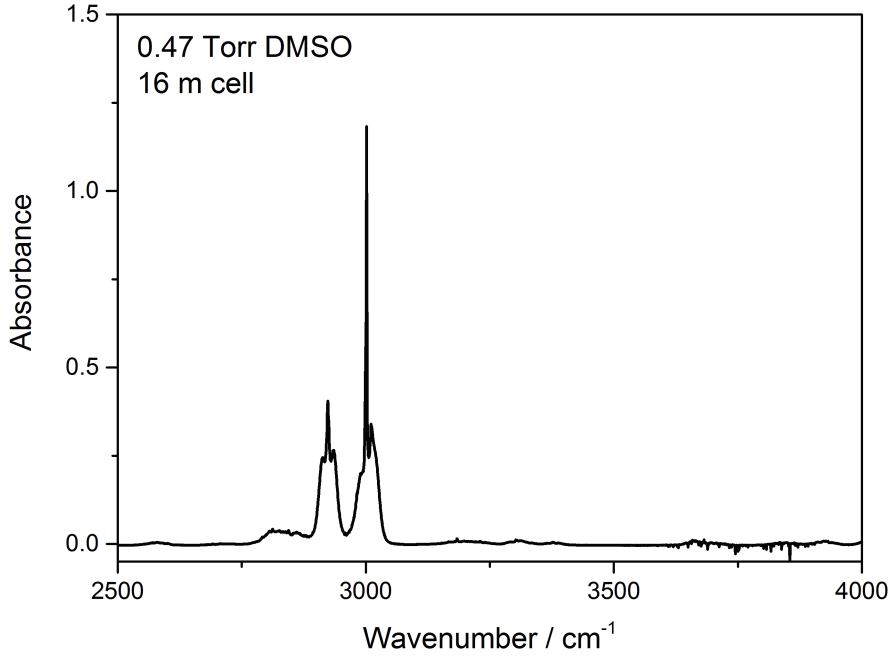

Figure S10: Spectrum of gas phase DMSO monomer in the 2500 - 4000 cm^{-1} region.

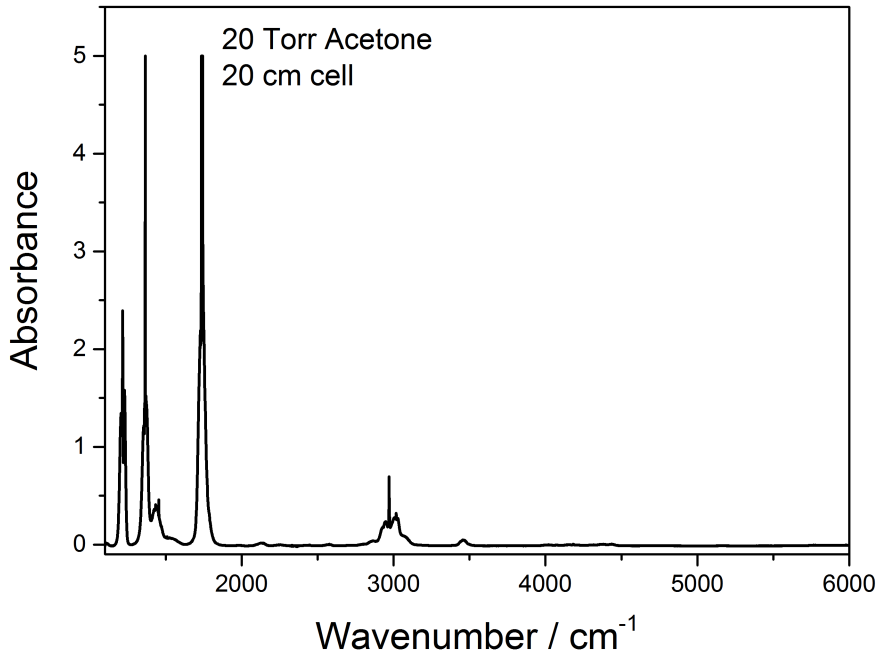

Figure S11: Spectrum of gas phase acetone monomer in the 1100 - 6000 cm^{-1} region.

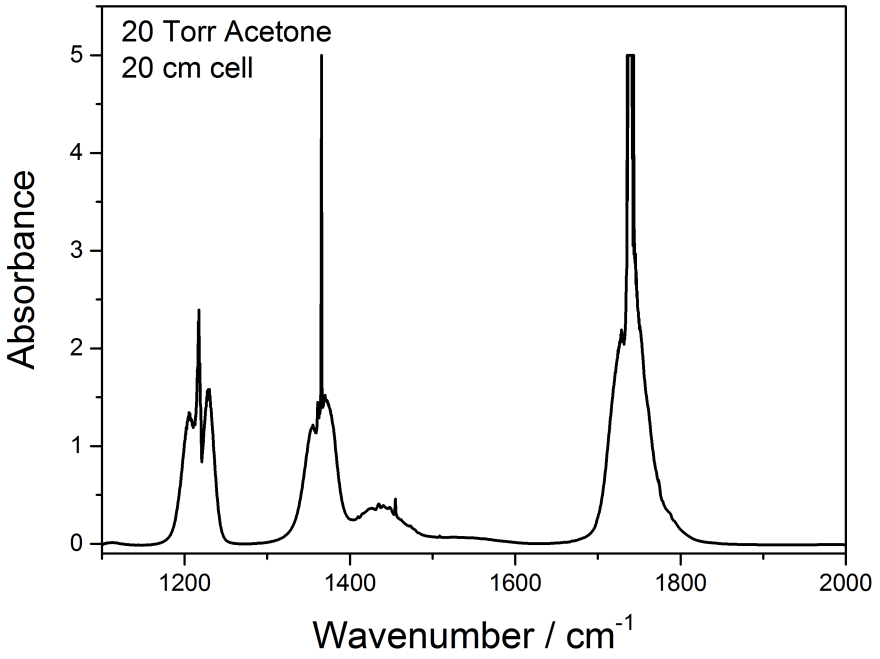

Figure S12: Spectrum of gas phase acetone monomer in the 1100 - 2000 cm^{-1} region.

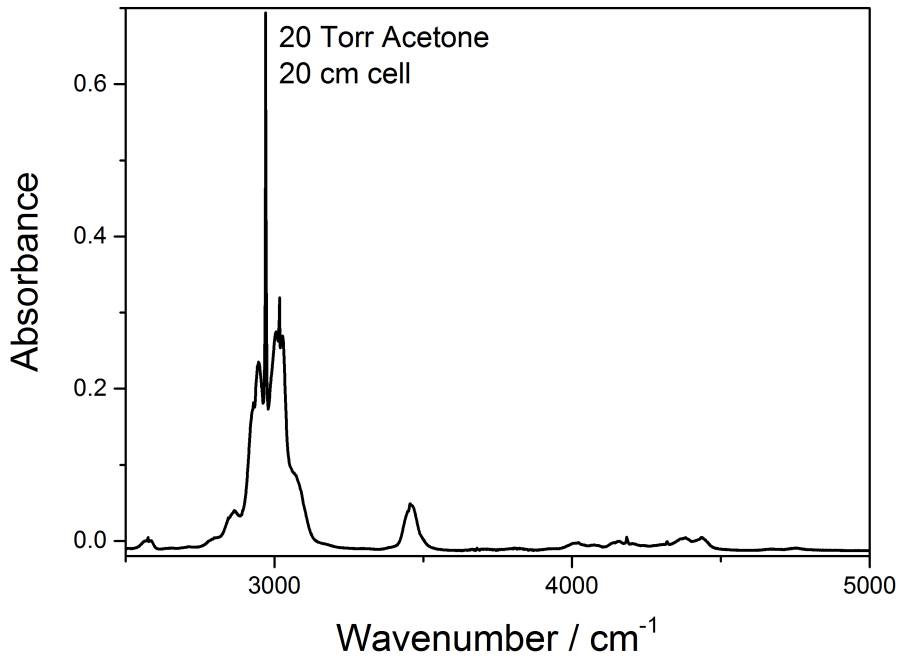

Figure S13: Spectrum of gas phase acetone monomer in the 2500 - 5000 cm^{-1} region.

S1.4 Gas phase spectra of the DMSO complexes

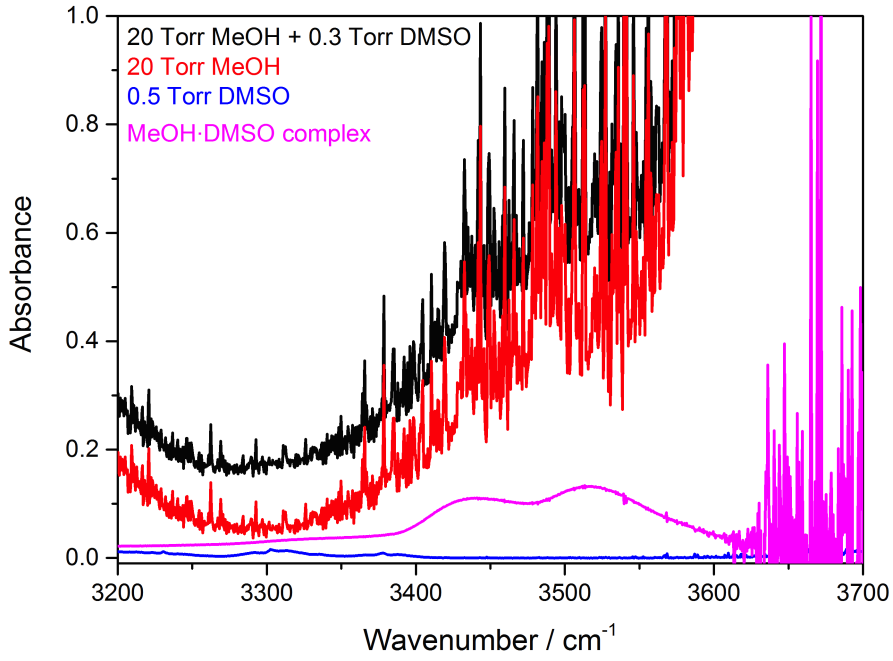

Figure S14: Spectra of MeOH + DMSO mixture (black) and the correponding monomers (red and blue). Spectra of the gas phase complex (pink) was obtained by subtracting the individual monomer spectra from the spectrum of the mixture. The spectra were recorded with a 16 m path length cell. For clarity the spectra have been offset.

MeOH also forms a dimer. At our conditions the MeOH dimer band is centered around 3599 cm^{-1} with a width of about 45 cm^{-1}, as shown in Figure 4 (and Figure S3, notice there is an error in this caption to S3, all 1 cm path lengths should be 10 cm) of reference 12. This is at the edge of the observed MeOH·DMSO band and would thus not affect the observed band significantly. In addition, the reference spectrum that is used to subtract the MeOH spectrum from that of the mixture is recorded at pressure close the MeOH pressure in the mixture. Thus the amount of MeOH dimer in the spectrum of the mixture and that of MeOH monomer will be very similar and spectral subtraction will eliminate most of the signal from the MeOH dimer. For the experiment with the highest MeOH pressure (Expt. H, 20 Torr) the scaling factor was 1.0 indicating that the MeOH reference spectrum had the same MeOH pressure as in the mixture and the effect of MeOH dimer on the MeOH·DMSO

spectrum will be minimal. Based on the MeOH dimer spectra in the previous work[12] we can estimate the absorbance from the MeOH dimer at a MeOH pressure of 20 Torr to be about 0.25 in the 16 meter cell used here. Even if the MeOH pressure differed by 1 Torr this would lead to a MeOH dimer absorbance of only 0.025 and thus still have very little effect on the MeOH·DMSO spectrum.

Table S2: The MeOH and DMSO pressures (Torr) used in the experiments for the mixtures and the integrated absorbance (cm^{-1}) of the observed OH-stretching bands. The MeOH pressure (Torr) used in the monomer spectra and the scaling factors (s.f.) used for the subtraction are also given.

	Mixture			Monomer	
Mix.	P_{MeOH}	P_{DMSO}	Int. Abs[b]	P_{MeOH}	s.f.
A[a]	3.24	0.35	2.93	3.91	0.83
B	6.16	0.30	5.08	5.50	1.12
C[a]	10.9	0.17	5.43	11.0	0.99
D	9.68	0.28	6.46	10.3	0.94
E	11.0	0.31	7.13	10.2	1.08
F[a]	14.7	0.26	10.1	12.1	1
G[a]	17.4	0.26	12.1	17.8	0.98
H[a]	20.2	0.29	14.8	20.2	1

a: Included in Figure 2.
b: Integrated from 3200 cm^{-1} to 3615 cm^{-1}.

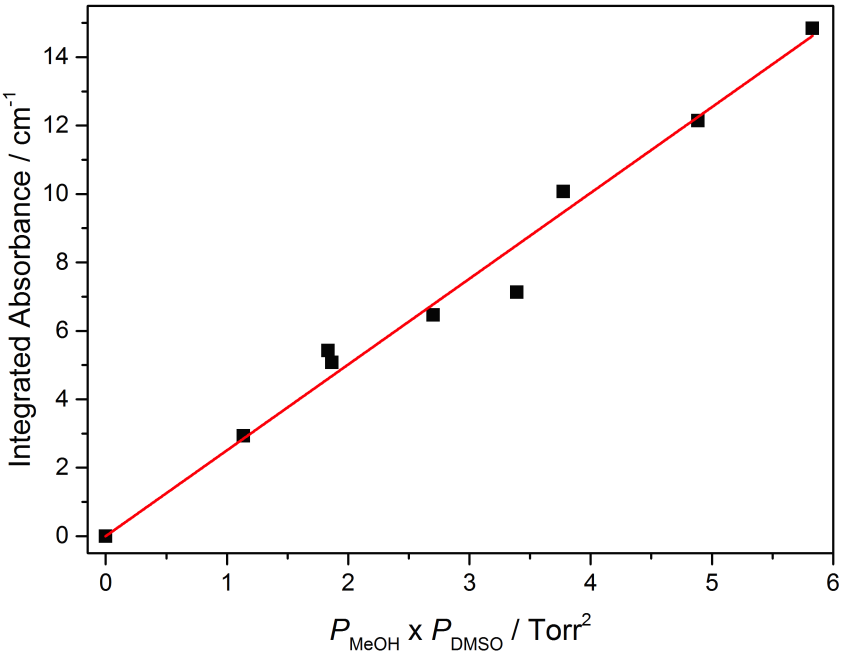

Figure S15: The integrated absorbance of the bands in the OH-stretching region plotted against the multiplied monomer pressures. A linear correlation is observed, which indicates the formation of a binary complex. The experimental details are listed in Tabel S2.

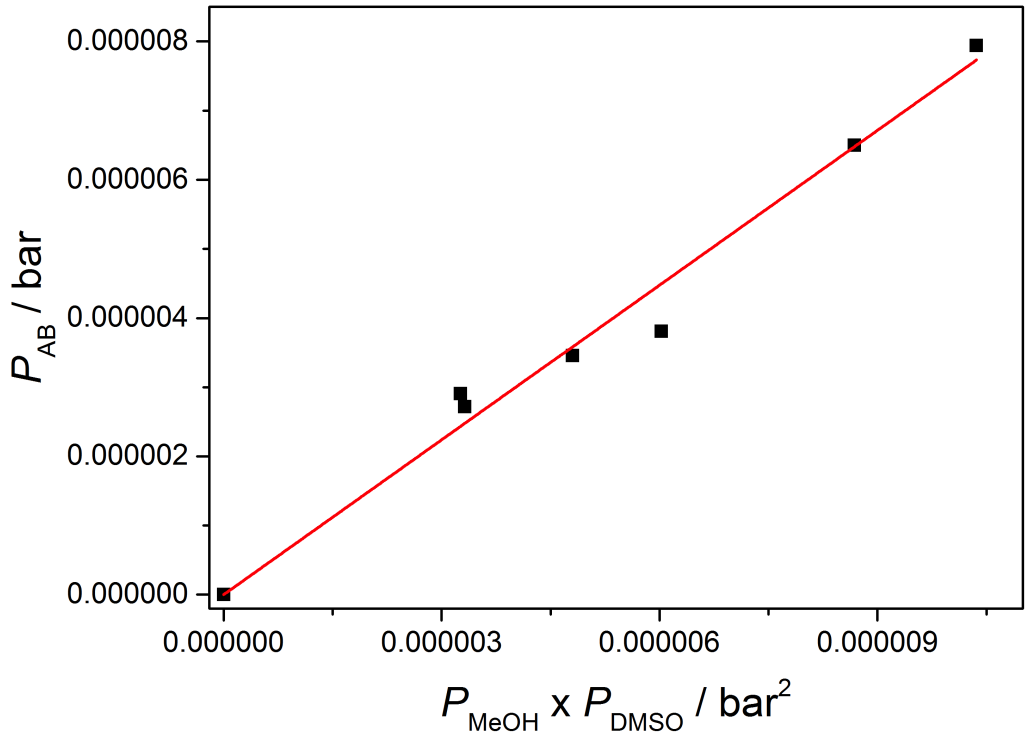

Figure S16: Pressure of the complexes plotted as a function of the multiplied monomer pressures. The K_P value is obtained from the slope of the fits. An oscillator strength of 1.09×10^{-4} was used.

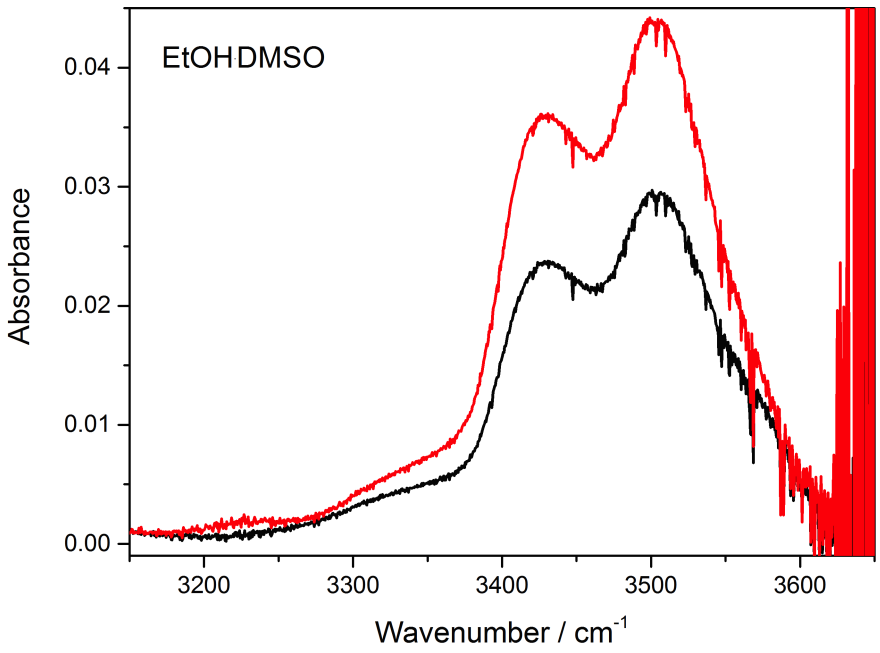

Figure S17: The OH-stretching vibration in the EtOH·DMSO complex. The red and black specta were recorded with monomer pressures of 10.5 Torr EtOH + 0.24 Torr DMSO and 5.67 Torr EtOH + 0.26 Torr DMSO, respectively. The spectra were recorded with a 16 m path length cell.

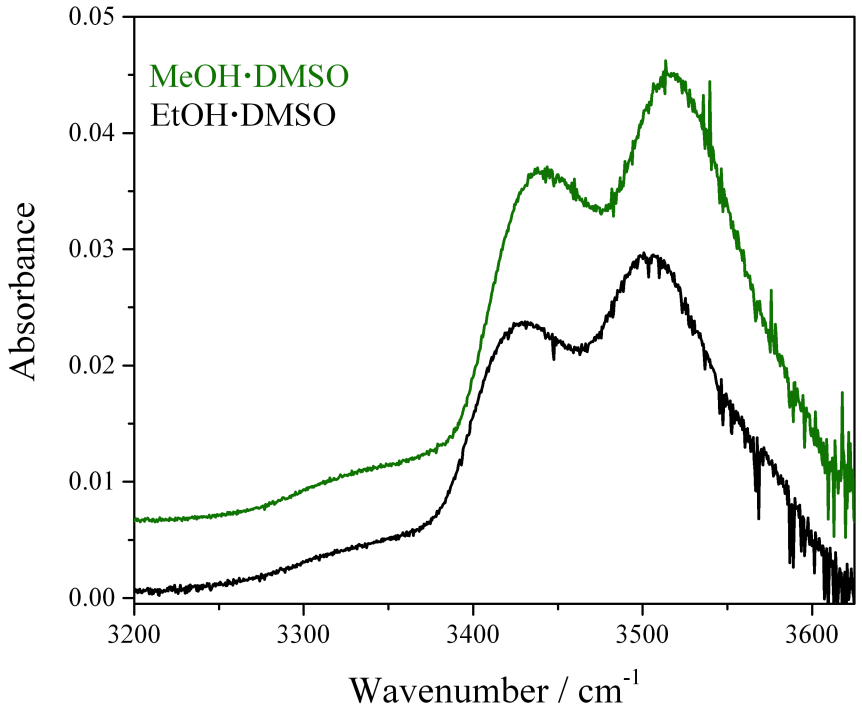

Figure S18: Comparison of the OH-stretching region in the MeOH·DMSO (green) and EtOH·DMSO (black) complexes. The spectra were recorded with a 16 m path length cell and with pressures: 11 Torr MeOH + 0.2 Torr DMSO and 6 Torr EtOH + 0.3 Torr DMSO.

As MeOH and DMSO were mixed we observed a redshift in the OH-stretching vibration compared to that of the isolated MeOH monomer. Other vibrations may also be effected by the MeOH·DMSO complexation. The effect on the SO-stretching vibration in DMSO has previously been investigated in solution.[13–15] The SO-stretching vibration in pure liquid DMSO was observed at 1050 cm^{-1}.[13] As liquid MeOH was added, the SO-stretching vibration shifted to 1022 cm^{-1}. The effect on the SO-stretching vibration was found to be solvent depended, and both redshifts and blueshifts of the SO-stretching vibration were observed when different organic solvents were added to liquid DMSO.[13] Redshifts of the SO-stretching vibration have also been observed as DMSO was dissolved in water and ascorbic acid.[14,15] In Table S3, we summarize the B3LYP/aug-cc-pVTZ normal mode SO-stretching vibration of DMSO and the MeOH·DMSO complex. For the strongest bound conformers, MD1 and MD2, the SO-stretching vibration is redshifted by $\sim$30 cm^{-1} upon complexation. The SO-stretching vibration in MD3 is hardly effected by the complexation, which is not surprising,

as it is not directly involved in the complex formation. For MD4, the SO-stretching vibration is redshifted by 10 cm^{-1} upon complexation. The observed frequencies are expected to be even smaller than the calculated values, as they are normal mode frequencies, which lack anharmonicity.

Table S3: Calculated B3LYP/aug-cc-pVTZ normal mode SO-stretching frequencies (cm^{-1}), redshifts (cm^{-1}), intensities and intensity ratios (f/f_{DMSO}) of DMSO and the MeOH·DMSO conformers.

Compound[a]	$\tilde{\nu}_{SO}$	f	$\Delta\tilde{\nu}_{SO}$	f/f_{DMSO}
DMSO	1080	2.6×10^{-5}	-	-
MD1	1050	3.8×10^{-5}	30	1.5
MD2	1049	4.2×10^{-5}	31	1.7
MD3	1087	1.0×10^{-5}	-7.5	0.4
MD4	1070	2.9×10^{-5}	10	1.2

a: Conformer abbreviations are defined in Figures 1 and S26.

The SO-stretching region of the gas phase MeOH·DMSO complex was investigated. Unfortunately, both DMSO and MeOH absorb strongly in the 750 - 1200 cm^{-1} region (Figures S6 and S9), caused by the SO-stretching vibration and OH-rocking, or a combination of COH-bend and CO-stretching, respectively. Low MeOH pressure (2.0 Torr in 16 m cell, KBr beam splitter) was therefore used. However, this leads to minimal complex formation. For comparison, 20 Torr MeOH and 0.29 Torr DMSO lead to only 0.0056 Torr of MeOH·DMSO complex. In Figure S19, we show a spectrum of a 2.0 Torr MeOH + 0.18 Torr DMSO mixture (red) and a spectrum of the MeOH·DMSO complex (black) were the individual monomer spectra have been subtracted from the mixture.[16] In part A and B of the figure, we present the SO-stretching and OH-stretching regions, respectively. In some regions of the spectrum of the complex noise is present (1000 - 1100 cm^{-1} and 3700 cm^{-1}), which is caused by saturation from MeOH and DMSO. No clear bands are observed in the spectrum of the complex in the SO-stretching region. The characteristic OH-stretching vibration of the MeOH·DMSO complex, shown in Figure 2, is not observed in the black spectrum in Figure S19B. This

indicates that only a very small amount of complex is formed. A similar experiment was performed with higher MeOH pressure (20 Torr) shown in Figure S20. However, the vibrational transition from MeOH in the 750 - 1200 cm^{-1} region saturates, and no bands from the MeOH·DMSO complex are observed in the SO-stretching region, see Figure S20A. In the OH-stretching region, the characteristic OH-stretching vibration is observed; however, the absorbance is very weak. In order to use higher MeOH pressure, a shorter optical path length was used (2.4 m), which has the drawback that a lower signal is obtained. In Figure S21, spectra of the MeOH monomer in the 750 - 1200 cm^{-1} region are shown. Even with shorter optical path lengths, the absorbance from MeOH in the 750 - 1200 cm^{-1} region saturates, and no peaks from the MeOH·DMSO complex can be observed in the SO-stretching region. The OH-stretching vibration in the MeOH·DMSO complex was observed with the 2.4 m cell (Figure S22), though the absorbance was very low. In conclusion, we were unable to detect the SO-stretching vibration in the gas phase MeOH·DMSO complex, due to the low frequency shift and the small amount of MeOH·DMSO complex formed.

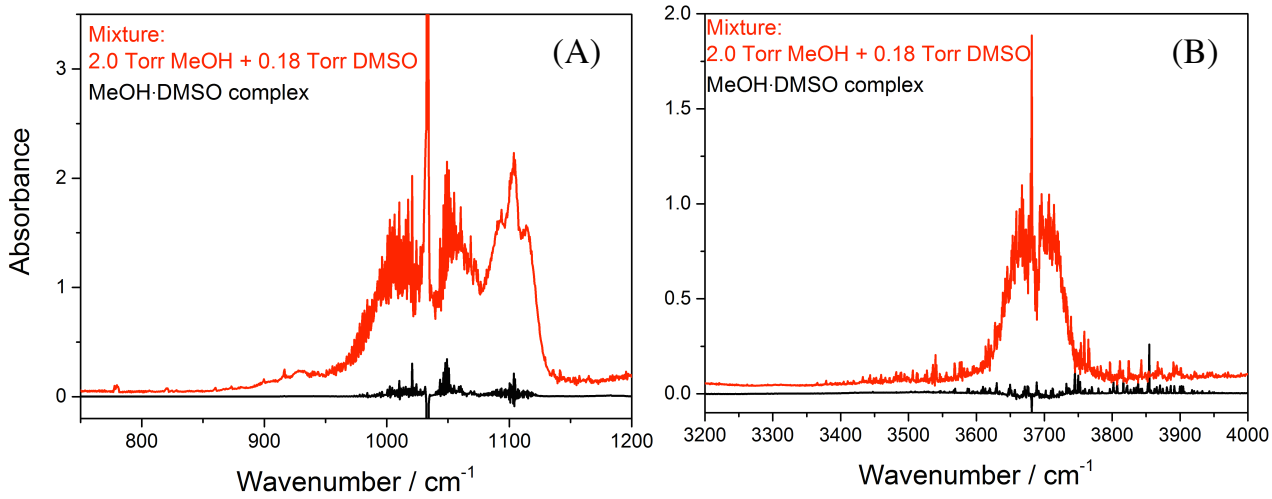

Figure S19: Spectra of a 2.0 Torr MeOH + 0.18 Torr DMSO mixture (red) and of the MeOH·DMSO complex (black) where the individual monomer spectra have been subtracted from the mixture.[12,16–21] In part A and B of the figure, the vibrations of the SO-stretching and OH-stretching regions are shown, respectively. The spectra were recorded with a 16 m path length cell.

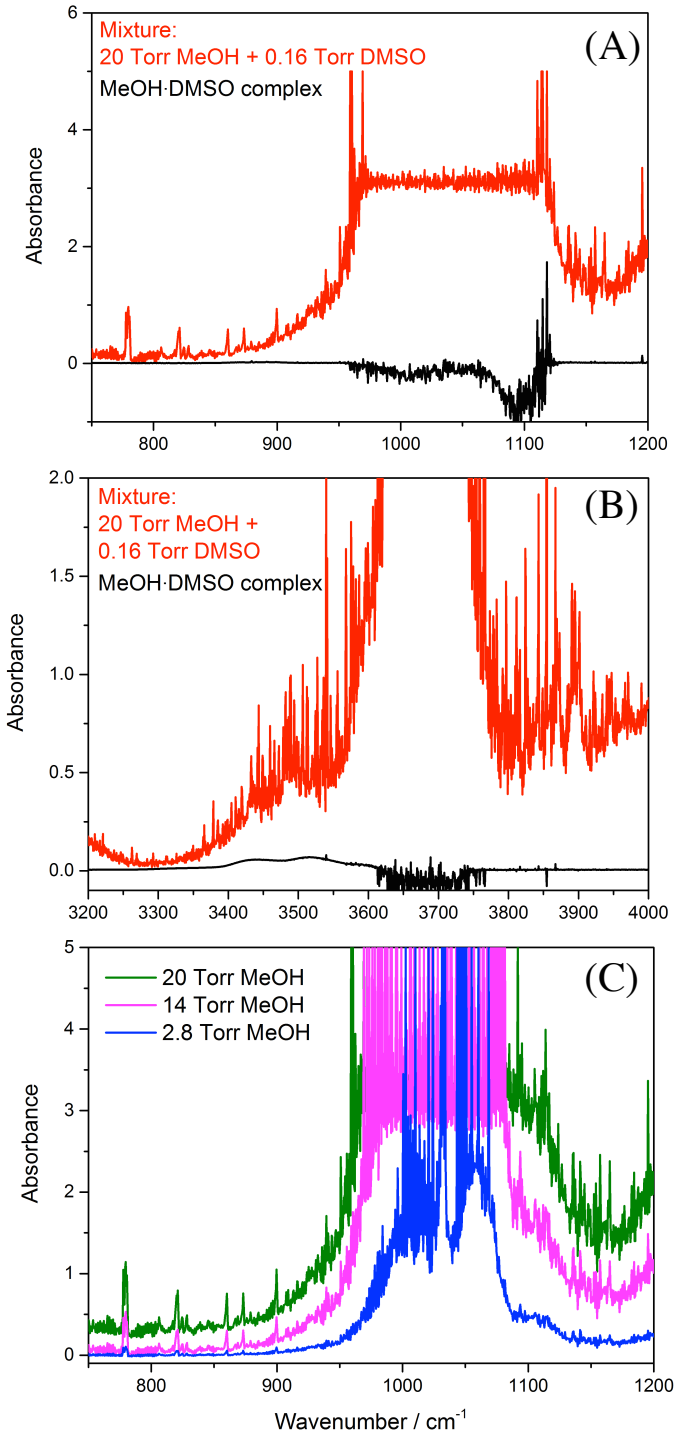

Figure S20: Spectrum of a MeOH and DMSO mixture (red) and a spectrum of the MeOH·DMSO complex (black) in the SO- and OH-stretching regions. Spectra of the MeOH monomer in the SO-stretching region is also shown to illustrate how MeOH saturates this region. All spectra were recorded with a 16 m cell.

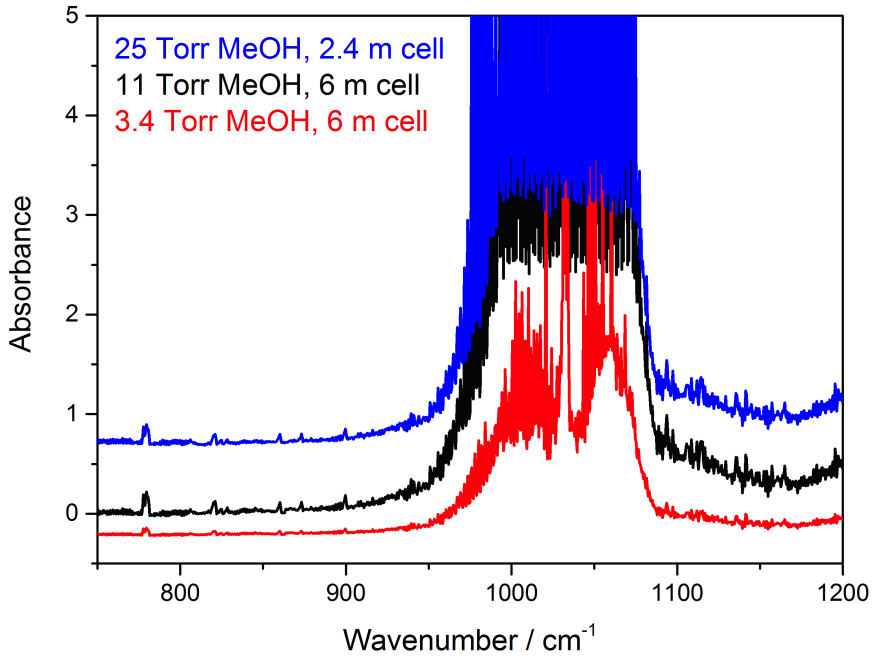

Figure S21: Spectra of the MeOH monomer in the SO-stretching region recorded with 2.4 and 6 m cells. The spectra illustrate how MeOH saturates the SO-stretching region.

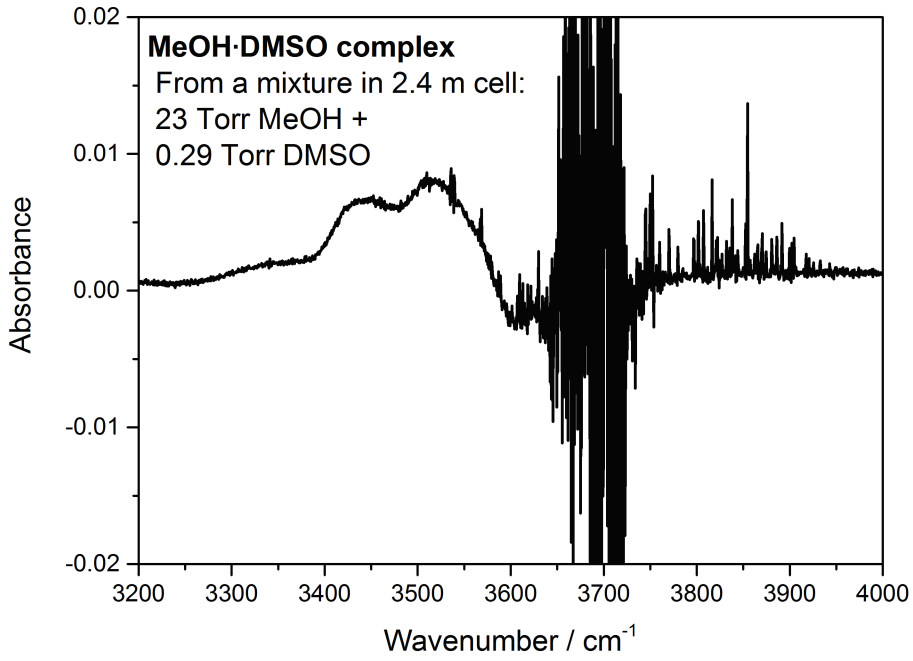

Figure S22: Spectrum of the MeOH·DMSO complex in the OH-stretching region. The spectrum was recorded with a 2.4 m cell. The two characteristic peaks in the OH-stretching region are observed.

S1.5 Gas phase spectra of the acetone complexes

In addition to the previous detection of the MeOH·acetone complex with matrix isolation spectroscopy,[11] the complex has also been detected in the gas phase at room temperature and under jet cooled conditions.[22,23] In the matrix isolation spectra, two peaks (3503 and 3518 cm^{-1}) were observed for the hydrogen bound complex, which was attributed to two different conformers. In the previous room temperature gas phase spectra one peak was observed at 3598 cm^{-1}.[22] In our gas phase room temperature spectra, two adjacent peaks are observed, which both arise from the binary MeOH·acetone complex. The observed spectrum was fitted with two Gaussian functions and indicates the presence of two transitions. The previous band position (3598 cm^{-1}) reported at room temperature for the OH-stretching vibration in the MeOH·acetone complex is close to the band center ($\sim$3595 cm^{-1}) observed in our spectrum. The detection of two peaks in our room temperature measurements could be caused by an improved resolution compared to the previous measurement where only one peak was observed. Under jet cooled conditions, the OH-stretching transition is observed at 3530 cm^{-1}, which is $\sim$60 cm^{-1} lower than that in our room temperature spectrum. With the 2D+2D LMPT model and the CCSD(T)- F12a/VDZ-F12 level of theory the calculated OH-stretching frequency of the MeOH·acetone complex is 3537 cm^{-1}, see Table S7. We expect the calculated frequency to be slightly lower than the observed frequency for measurements performed in the gas phase at room temperature.[24]

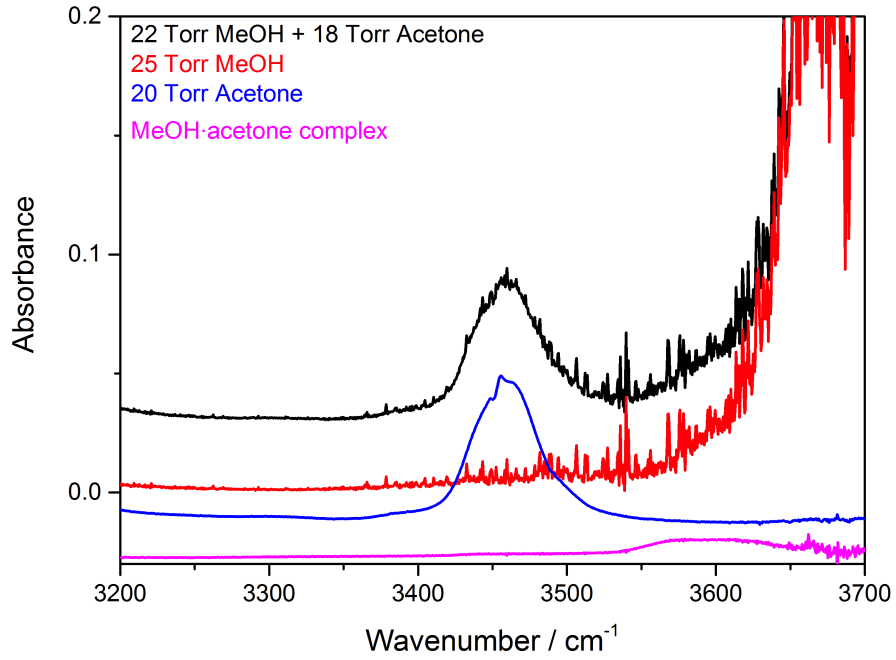

Figure S23: Spectra of MeOH + acetone mixture (black) and the correponding monomers (red and blue). Spectra of the gas phase complex (pink) was obtained by subtracting the individual monomer spectra from the spectrum of the mixture. The spectra were recorded with a 20 cm path length cell. For clarity the spectra have been offset.

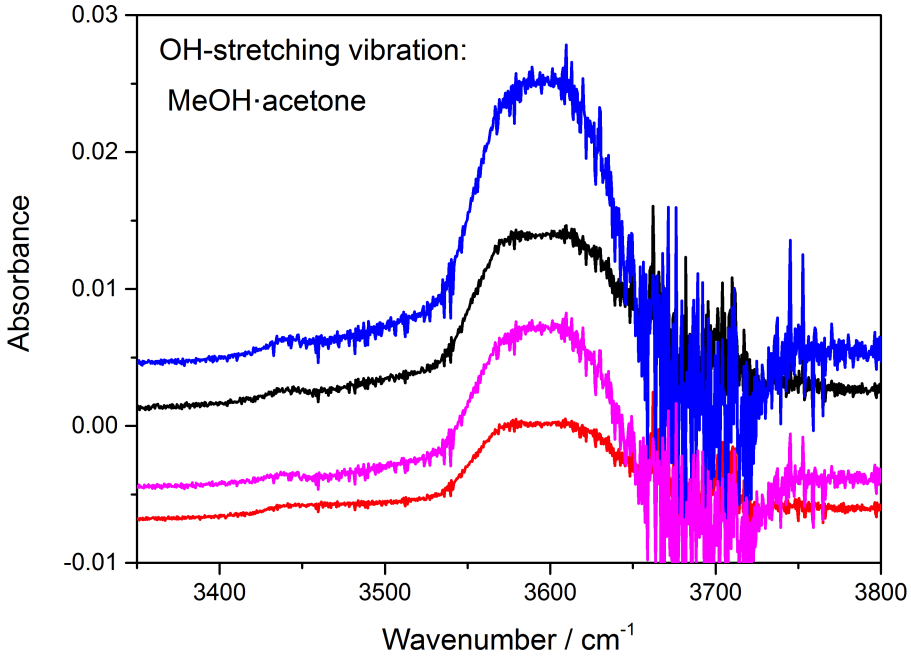

Figure S24: Spectra of the OH-stretching region in the MeOH·acetone complex. The pressures used in each measurement are given in Table S4.

Table S4: The MeOH and acetone pressures (Torr) used in the experiments and the integrated absorbance (cm^{-1}) of the observed OH-stretching bands.

	Mixture			Monomer	
Mix.	P_{MeOH}	$P_{Acetone}$	Int. Abs[a]	P_{MeOH}	s.f.
A	23.1	50.7	1.24	23.1	1
B	28.4	24.1	0.698	32.7	1.2
C	17.0	37.8	0.739	17.0	1
D	21.7	17.9	0.364	24.9	0.9

a: Integrated from 3500 cm^{-1} to 3670 cm^{-1}.

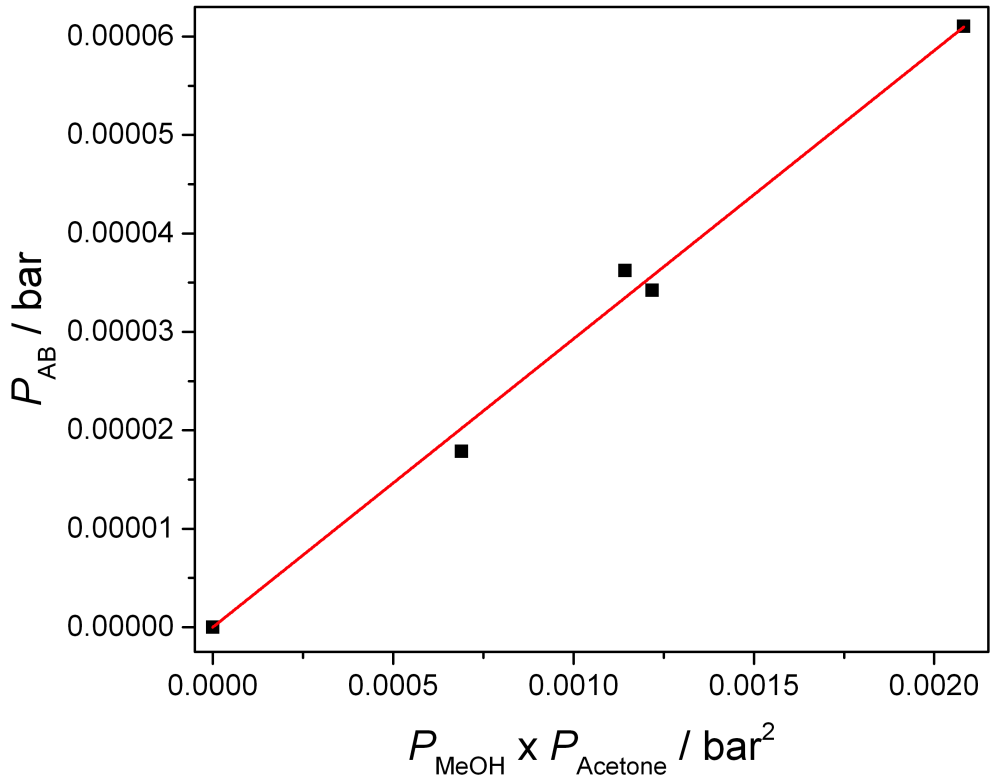

Figure S25: Pressure of the complexes plotted as a function of the multiplied monomer pressures. K_P is obtained from the slope of the fits. An oscillator strength of 1.09×10^{-4} was used.

S2 Theoretical results

S2.1 Local Mode Perturbation Theory

The displacement coordinates of the OH-stretching and the COH-bending oscillators are q_{b} and θ, respectively. The one dimensional (1D) potential for the OH-stretch, $V(q_{\mathrm{b}})$, is obtained by displacing the OH bond by -0.40 Å to +0.70 Å in steps of 0.05 Å from the equilibrium structure. For the COH-bending oscillator [$V(\theta)$] the COH angle is displaced by -50 degrees to +80 degrees in the steps of 5 degrees. The two dimensional (2D) potential energy surface, $V(q_{\mathrm{b}}, \theta)$, is obtained by simultaneously displacing the OH-stretch and COH-bend.[24–26] In this case, the displacements are from -0.20 Å to +0.20 Å in steps of 0.05 Å for the OH-stretch, and from -20 degrees to +20 degrees in steps of 5 degrees for the COH-bend. The two intermolecular modes (donor rock, β, and the donor twist, x,) are treated as harmonic oscillators, and the harmonic frequency is determined via the second derivative of 1D potential energy surfaces obtained by displacing each intermolecular mode by -20 degrees to +20 degrees in the steps of 5 degrees. Rayleigh-Schrödinger Perturbation theory is applied to include the effect of the two intermolecular modes on the donor vibrations. Each of the donor vibrations are coupled through the potential energy surface to each of the two intermolecular modes.[24–26] The displacement of the OH bond is from -0.20 Å to +0.20 Å in steps of 0.05 Å, and for the other modes the displacement is from -20 degrees to +20 degrees in steps of 5 degrees.

S2.2 Complexes with MeOH as hydrogen bond donor

MeOH·DMSO:

In Figure S26, we show the higher energy conformer of the MeOH·DMSO complex. The MeOH·DMSO MD1 and MD2 conformers have previously been identified theoretically.[27] The corresponding calculated binding energies are given in Table S5. For the MeOH·DMSO complex, four conformers were found; two with an OH$\cdots$O hydrogen bond (MD1 and MD2), one with an OH$\cdots$S hydrogen bond (MD3) and one with a CH$\cdots$O hydrogen bond (MD4). MD1 and MD2, shown in Figure 1, are the strongest hydrogen bound conformers with binding energies of approximately -40 kJ/mol. The binding energy of the weaker bound conformers, MD3 and MD4, is approximately -19 kJ/mol. Based on the electronegativity of the carbon (2.5) and oxygen (3.5) atoms, we expect the hydrogen bound conformer with a CH donor group, to be weaker than the conformers with an OH donor group. This is also predicted from the calculated binding energies of MD1, MD2 and MD4. However, we find that MD3, with an OH$\cdots$S hydrogen bond, is $\sim$20 kJ/mol weaker bound than MD1 and MD2, even though previous investigations of the OH$\cdots$S and OH$\cdots$O type of hydrogen bound complexes, with dimethyl sulfide and dimethyl ether as hydrogen bond acceptors, found them to be of similar strength.[12,28,29] Due to the neighbouring oxygen atom in DMSO, the sulphur atom is less electron rich compared to the sulphur atom in dimethyl sulfide. The oxygen atom in DMSO is also more accessible than the sulphur atom, which is shielded by the methyl groups. Hence, the oxygen atom can more easily engage in a hydrogen bond interaction compared to the sulphur atom, and thereby acts as a stronger hydrogen bond acceptor. The strength of a hydrogen bound complex is often estimated from the hydrogen bond angle and the elongation of the XH bond length upon complexation.[30] An angle close to 180° and a large elongation indicate a strong hydrogen bond.[30] For MD3 and MD4, we find that MD3 has the largest XH bond length elongation, whereas MD4 has a hydrogen bond angle closest to 180°. Hence, the two parameters are contradicting, and the determination

of hydrogen bond strengths based on the calculated geometric parameters, should be done tentatively. However, hydrogen bound complexes with a CH group as the donor are known to blueshift upon complexation,[17,18] and only a small elongation of the CH bond length is found for the MD4 conformer.

As seen from Table S5, not all DFT functionals are able to re-optimize the CCSD(T)-F12a/VDZ-F12 MeOH·DMSO conformers. In general the B3LYP functional underestimates the binding energies with ∼8 kJ/mol for all conformers, compared to the CCSD(T)-F12a/VDZ-F12 method. The other three functionals all reproduce the CCSD(T)-F12a/VDZ-F12 binding energies within 3 kJ/mol. However, if we compare the DFT geometric parameters of the optimized structures, with the values obtained at the CCSD(T)-F12a/VDZ-F12 level of theory, we find that all functionals, including B3LYP, reproduce the CCSD(T)-F12a/VDZ-F12 values.[19]

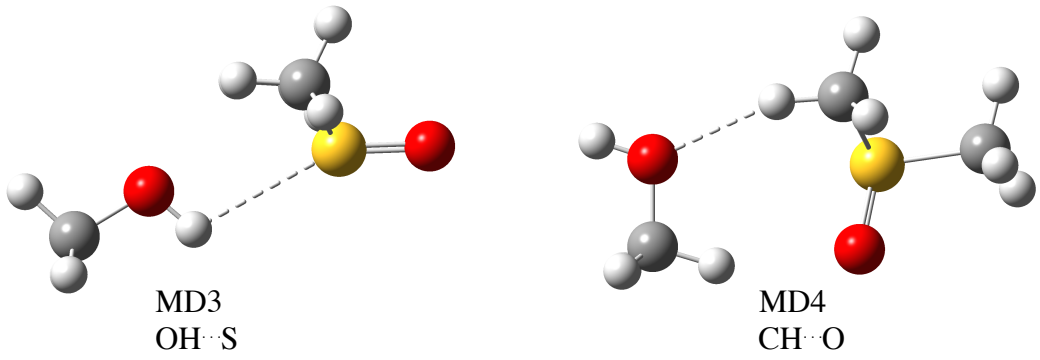

Figure S26: CCSD(T)-F12a/VDZ-F12 optimized structures of the MeOH·DMSO (MD3, C_s and MD4, C_1) high energy conformers. The MD4 conformer can be interconverted by symmetry and has a degeneracy of 2.

Table S5: Calculated electronic binding energies (E_e in kJ/mol), zero point vibrational correction (ZPVE in kJ/mol), ZPVE corrected electronic binding energies (BE in kJ/mol) and optimized geometric parameters (Å and degrees) for the MeOH·DMSO conformers.[a]

	BE	E_e	ZPVE	ΔR_{XH}	R_{HB}	θ_{HB}
CCSD(T)-F12a:						
MD1	-	-42.9	-	0.0110	1.87	161
MD2	-	-36.9	-	0.0146	1.84	159
MD3	-	-19.3	-	0.0028	2.71	111
MD4	-	-19.4	-	0.0007	2.29	155
B3LYP:						
MD1	-28.1	-34.0	5.88	0.0161	1.84	160
MD2	-24.2	-29.2	5.01	0.0123	1.87	163
MD3	-7.53	-10.6	3.09	0.0022	2.81	113
MD4	-8.03	-11.4	3.38	0.0009	2.38	160
B3LYP-D3:						
MD1	-39.3	-46.0	6.74	0.0165	1.83	159
MD2[b]	-	-	-	-	-	-
MD3	-15.9	-19.7	3.79	0.0021	2.84	108
MD4	-17.1	-20.8	3.75	0.0002	2.31	155
ωB97X-D:						
MD1	-36.8	-43.3	6.47	0.0169	1.82	160
MD2[b]	-	-	-	-	-	-
MD3	-14.3	-17.8	3.52	0.0031	2.71	114
MD4	-14.3	-17.8	3.49	0.0017	2.27	161
M06-2X:						
MD1	-40.5	-46.7	6.17	0.0167	1.81	158
MD2	-33.7	-38.9	5.22	0.0125	1.86	158
MD3	-16.8	-20.5	3.76	0.0029	2.70	107
MD4[c]	-	-	-	-	-	-
MP2:						
MD1	-40.8	-47.8	6.25	0.0179	1.80	160
MD2	-34.4	-39.8	5.36	0.0134	1.84	161
MD3	-18.1	-21.7	3.55	0.0031	2.68	111
MD4	-18.6	-21.9	3.33	0.0002	2.32	144

a: Calculated with CCSD(T)-F12a/VDZ-F12, DFT/aug-cc-pVTZ and MP2/aug-cc-pVTZ methods.
b: Terminated as MD1.
c: Terminated as MD2.

MeOH·acetone:

In Figure S27, we show the MeOH·acetone conformers and the corresponding calculated binding energies are given in Table S6. The MeOH·acetone MA1 conformer has previously been identified theoretically.[11,23,27] Three conformers were found with the CCSD(T)-F12a/VDZ-F12 method. MA1 and MA4 were re-optimized with the B3LYP, B3LYP-D, ωB97X-D and M06-2X functionals, whereas MA3 could only be optimized with the M06-2X functional. An additional conformer (MA2) was found with the ωB97X-D and M06-2X functionals, see Figure S27. In a previous investigation of the MeOH·acetone complex, the hydrogen bond angle in MA1 was changed to find additional stable conformers of the complex.[11] A structure with an angle of 150° was found. We were unable to optimize this structure; however, the MA2 conformer (only found with ωB97X-D and M06-2X) is similar in energy to MA1.

A stronger interaction between MeOH and DMSO is predicted compared to that between MeOH and acetone by approximately 8 - 14 kJ/mol. In addition, the OH bond length of MeOH is elongated more in the MeOH·DMSO complex compared to in MeOH·acetone, which supports the larger OH-stretching redshift observed for the MeOH·DMSO complex.

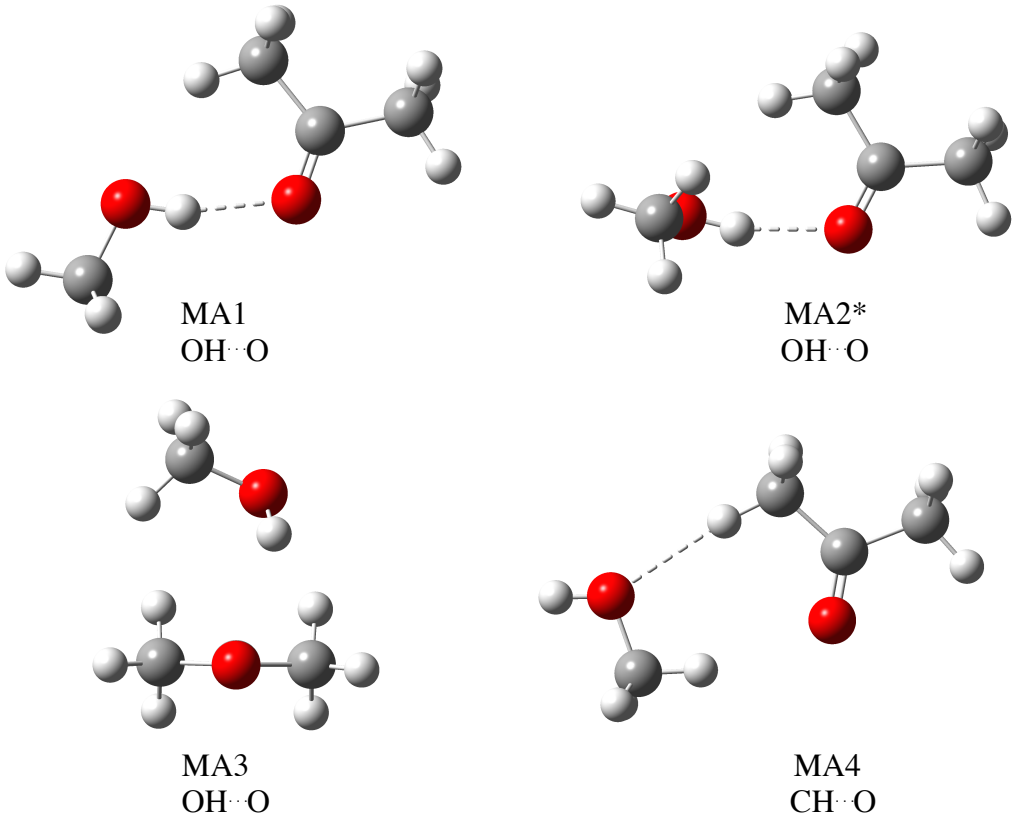

Figure S27: CCSD(T)-F12a/VDZ-F12 optimized structures of the MeOH·acetone conformers. The MA2* conformer shown was optimized with the ωB97X-D/aug-cc-pVTZ method. The MA3 and MA2* conformers have a symmetry factor of 4 while conformers MA1 and MA4 have a symmetry factor of 2. The conformer was not optimized with the CCSD(T)-F12a/VDZ-F12 method, which is indicated by the asterisk.

Table S6: Calculated electronic binding energies (E_e in kJ/mol), zero point vibrational correction (ZPVE in kJ/mol), ZPVE corrected electronic binding energies (BE in kJ/mol) and optimized geometric parameters (Å and degrees) for the MeOH·acetone conformers.[a]

	BE	E_e	ZPVE	ΔR_{XH}	R_{HB}	θ_{HB}
CCSD(T)-F12a:						
MA1	-	-29.1	-	0.0088	1.90	166
MA2[b]	-	-	-	-	-	
MA3	-	-20.8	-	0.0031	2.32	131
MA4	-	-13.3	-	0.0006	2.36	173
B3LYP:						
MA1	-18.2	-23.3	5.18	0.0097	1.91	166
MA2[b]	-	-	-	-	-	-
MA3[b]	-	-	-	-	-	-
MA4	-3.99	-7.00	3.02	0.0002	2.49	172
B3LYP-D3:						
MA1	-25.3	-30.8	5.51	0.0100	1.89	165
MA2[b]	-	-	-	-	-	-
MA3[b]	-	-	-	-	-	-
MA4	10.3	7.43	3.00	0.0002	2.49	172
ωB97X-D:						
MA1	-23.2	-28.8	5.55	0.0106	1.89	167
MA2	-22.9	-28.7	5.72	0.0101	1.92	165
MA3[b]	-	-	-	-	-	-
MA4	-8.84	-12.3	3.49	0.0007	2.38	175
M06-2X:						
MA1	-24.1	-29.3	5.23	0.0092	1.90	163
MA2	-23.3	-28.8	5.53	0.0081	1.94	159
MA3	-19.6	-24.5	4.89	0.0029	2.42	118
MA4	-8.57	-11.7	3.29	0.0011	2.34	177
MP2:						
MA1	-25.3	-31.0	5.63	0.0101	1.88	166
MA2[b]	-	-	-	-	-	-
MA3[b]	-	-	-	-	-	-
MA4	-11.3	-14.6	3.38	0.0010	2.35	173

a: Calculated with CCSD(T)-F12a/VDZ-F12, DFT/aug-cc-pVTZ and MP2/aug-cc-pVTZ methods.
b: Unable to converge.

Table S7: Calculated fundamental OH-stretching frequencies ($\tilde{\nu}$ in cm^{-1}), redshifts ($\Delta\tilde{\nu}$ in cm^{-1}) and intensities (f) for the MeOH monomer and the MeOH·acetone complex.

	Calculated[a]		
Conformer	$\tilde{\nu}$	$\Delta\tilde{\nu}$[b]	f
MeOH	3683	-	3.59×10^{-6}
MA1	3537	146	1.09×10^{-4}

a: Calculated with the 2D+2D LMPT model and the CCSD(T)-F12a/VDZ-F12 method.[24] The MeOH monomer frequency is calculated with a 2D local mode model.
b: $\Delta\tilde{\nu} = \tilde{\nu}_{\text{Alcohol}}$ - $\tilde{\nu}_{\text{complex}}$.

Calculated abundances:

From the calculated Gibbs free energy ($G^{\ominus}_{298.15\mathrm{K}}$) we determine the abundances of the MeOH·DMSO conformers using the Boltzmann formalism. The abundance of a conformer M is:

$$F(\mathrm{M}) = \frac{g_{\mathrm{M}} \exp(-(G^{\ominus}_{0,298.15\mathrm{K}} - G^{\ominus}_{\mathrm{M},298.15\mathrm{K}})/N_A k_B T)}{\sum_i g_i \exp(-G^{\ominus}_{i,298.15\mathrm{K}}/N_A k_B T)}, \quad (1)$$

where i spans over all present conformers. g_{M} is the degeneracy of conformer M, N_A is Avogadro's constant, k_B is Boltzmann's constant and T is the temperature. Some of the conformers in Figures 1 and S26 have symmetry. We have optimized the structures with and without constraining the symmetry to investigate the effect on the calculated frequency, and hence the calculated Gibbs free energy values and thereby the abundance. We find that constraining the symmetry changes the calculated abundance with less than a few percent.

Table S8: Calculated abudance (%) of the MeOH·DMSO without constraining the symmetry.

	MeOH·DMSO			
Method	MD1	MD2	MD3	MD4
F12a//B3LYP:[a]	58	41	0.18	0.11
F12a//M06-2X:[a]	48	51	0.039	-[b]
M06-2X:	61	39	0.018	-[b]
ωB97X-D:	-	-[b]	-	-

a: F12a//DFT = CCSD(T)-F12a/VDZ-F12//DFT/aug-cc-pVTZ.
b: DFT structure not found.

S2.3 Complexes with H_2O as hydrogen bond donor

In Figure S28, we show the higher energy H_2O·DMSO conformer (HD3) and the H_2O·acetone conformer (HA1). In Table S9, the corresponding binding energies are given.

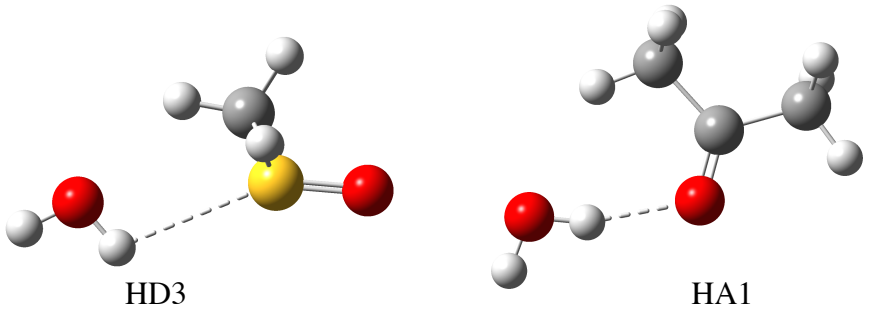

Figure S28: CCSD(T)-F12a/VDZ-F12 optimized structures of the H_2O·DMSO and H_2O·acetone conformers.

Table S9: Calculated electronic binding energies (E_e in kJ/mol), zero point vibrational correction (ZPVE in kJ/mol), ZPVE corrected electronic binding energies (BE in kJ/mol) and optimized geometric parameters (Å and degrees) for the H_2O·DMSO (HD) and H_2O·acetone (HA) conformers.[a]

Complex	BE	E_e	ZPVE	ΔR_{OH}	R_{HB}	θ_{HB}
CCSD(T)-F12a:						
HD1	-	-41.5	-	0.0152	1.84	157
HD2	-	-35.1	-	0.0116	1.88	160
HD3	-	-17.9	-	0.0027	2.76	109
HA1	-	-28.2	-	0.0094	1.91	164
B3LYP:						
HD1	-25.8	-34.3	8.55	0.0173	1.83	159
HD2	-21.8	-29.5	7.65	0.0134	1.87	162
HD3	-5.78	-10.4	4.60	0.0025	2.78	115
HA1	-16.2	-23.7	7.55	0.0107	1.91	166
B3LYP-D3:						
HD1	-35.4	-44.8	9.44	0.0176	1.83	158
HD2[b]	-	-	-	-	-	-
HD3	-12.8	-18.2	5.34	0.0022	2.84	108
HA1	-22.3	-30.3	7.92	0.0109	1.90	164
ωB97X-D:						
HD1	-32.5	-41.9	9.34	0.0177	1.83	159
HD2[b]	-	-	-	-	-	-
HD3	-11.4	-16.4	4.93	0.0032	2.71	114
HA1	-20.2	-27.9	7.67	0.0113	1.90	166
M06-2X:						
HD1	-37.7	-46.7	9.00	0.0178	1.81	157
HD2	-30.7	-38.8	8.04	0.0134	1.86	158
HD3	-14.9	-19.9	5.00	0.0030	2.70	106
HA1	-21.6	-29.4	7.78	0.0010	1.90	162
MP2:						
HD1	-35.7	-44.6	8.88	0.0185	1.81	158
HD2	-29.7	-37.7	7.98	0.0141	1.86	160
HD3	-14.3	-19.4	5.18	0.0030	2.72	109
HA1	-21.2	-29.3	8.05	0.0108	1.89	164

a: Calculated with CCSD(T)-F12a/VDZ-F12, DFT/aug-cc-pVTZ and MP2/aug-cc-pVTZ methods.
b: Unable to converge.

S2.4 Complexes with EtOH as hydrogen bond donor

In Figures S29 - S31, the B3LYP/aug-cc-pVTZ optimized structures of the EtOH·DMSO complex are shown. In Tables S10 and S11, the corresponding binding energies are given.

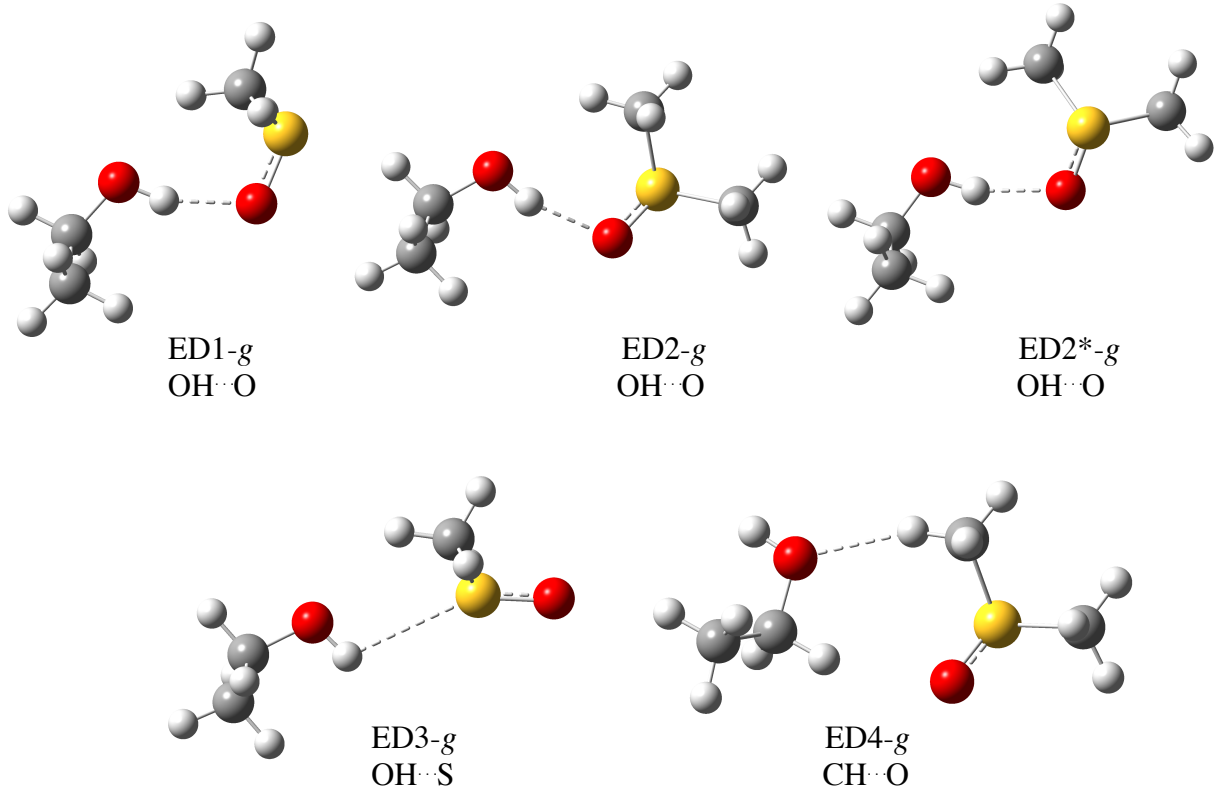

Figure S29: B3LYP/aug-cc-pVTZ optimized structures of the EtOH·DMSO conformers with EtOH in *gauche* configuration. The two ED2 structures are similar and one of them have been given an asterisk (ED2*-*g*) to distinguish between the two.

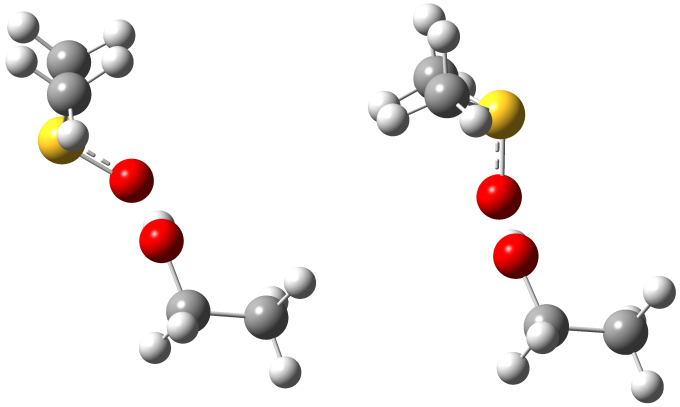

Figure S30: ED2 and ED2* B3LYP/aug-cc-pVTZ optimized conformers shown from a different angle. The asterisk is given to distinguish the two conformers.

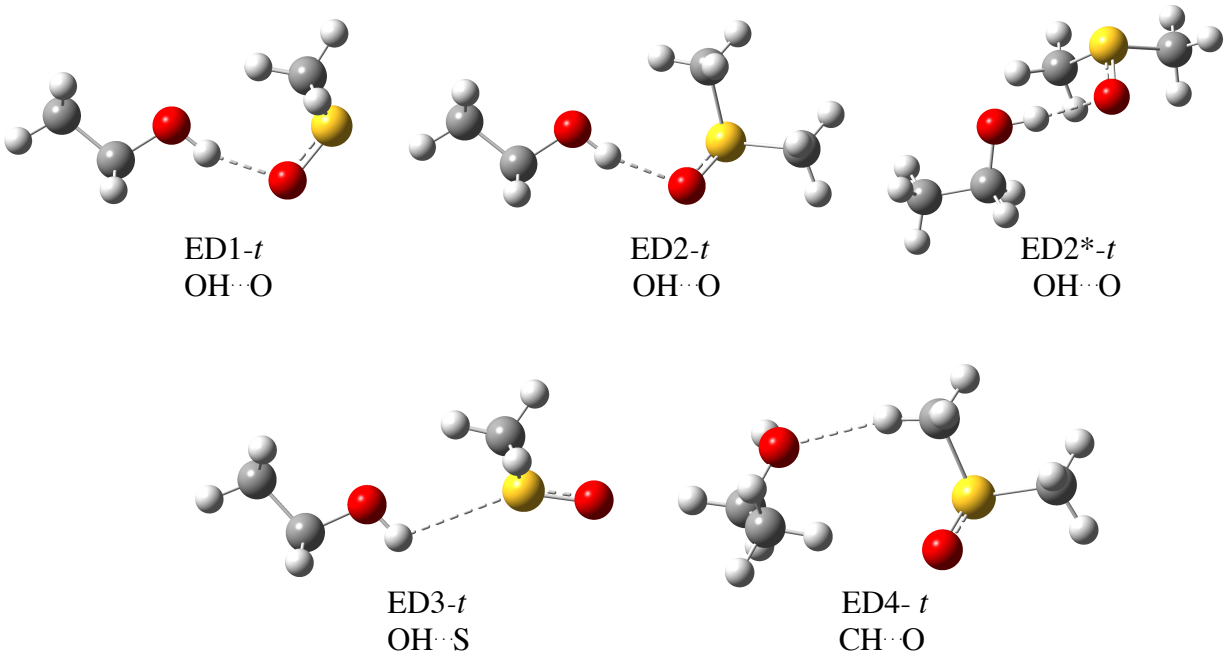

Figure S31: B3LYP/aug-cc-pVTZ optimized structures of the EtOH·DMSO with EtOH in *trans* configuration. The ED2*-*t* conformer shown was optimized with the MP2/aug-cc-pVTZ method.

Table S10: Calculated electronic binding energies (E_e in kJ/mol), zero point vibrational correction (ZPVE in kJ/mol), ZPVE corrected electronic binding energies (BE in kJ/mol) and optimized geometric parameters (Å and degrees) for the EtOH·DMSO (*gauche*) conformers.[a]

	BE	E_e	ZPVE	ΔR_{XH}	R_{HB}	θ_{HB}
B3LYP:						
ED1-*g*	-27.5	33.1	5.53	0.0152	1.85	160
ED2-*g*	-23.8	-28.4	4.68	0.0116	1.89	162
ED2*-*g*	-23.5	-28.2	4.68	0.0115	1.89	162
ED3-*g*	-7.92	-10.7	2.76	0.0091	2.87	111
ED4-*g*	-8.62	-11.5	2.83	0.0092	2.37	160
B3LYP-D3:						
ED1-*g*	-40.1	-46.7	6.68	0.0157	1.83	161
ED2-*g*[b]	-	-	-	-	-	-
ED2*-*g*	-32.7	-38.1	5.40	0.0112	1.88	162
ED3-*g*	-17.2	-20.8	3.58	0.0020	2.80	111
ED4-*g*	-19.4	-22.8	3.44	0.0006	2.32	157
ωB97X-D:						
ED1-*g*	-38.3	-44.7	6.45	0.0160	1.83	163
ED2-*g*[b]	-	-	-	-	-	-
ED2*-*g*	-30.9	-36.1	5.16	0.0117	1.88	163
ED3-*g*	-15.3	-19.6	4.32	0.0032	2.66	120
ED4-*g*	-16.4	-19.8	3.39	0.0022	2.29	163
M06-2X:						
ED1-*g*	-41.0	-47.4	6.43	0.0159	1.82	162
ED2-*g*[b]	-	-	-	-	-	-
ED2*-*g*	-32.7	-38.3	5.57	0.0106	1.89	158
ED3-*g*	-16.9	-20.7	3.81	0.0028	2.71	107
ED4-*g*	-16.2	-19.3	3.08	-0.0006	2.38	131
MP2:						
ED1-*g*	-42.7	-48.8	6.03	0.0175	1.80	163
ED2-*g*	-36.0	-40.9	4.95	0.0133	1.83	164
ED2*-*g*	-34.9	-39.9	4.98	0.0121	1.86	163
ED3-*g*	-19.8	-23.0	3.27	0.0033	2.62	117
ED4-*g*	-21.7	-24.2	2.27	0.0007	2.33	149

a: Calculated with CCSD(T)-F12a/VDZ-F12, DFT/aug-cc-pVTZ and MP2/aug-cc-pVTZ methods.
b: Terminated as ED1.

Table S11: Calculated electronic binding energies (E_e in kJ/mol), zero point vibrational correction (ZPVE in kJ/mol), ZPVE corrected electronic binding energies (BE in kJ/mol) and optimized geometric parameters (Å and degrees) for the EtOH·DMSO (*trans*) conformers.[a]

	BE	E_e	ZPVE	ΔR_{XH}	R_{HB}	θ_{HB}
B3LYP:						
ED1-*t*	-27.7	-33.1	5.33	0.0158	1.84	160
ED2-*t*	-23.9	-28.4	4.46	0.0121	1.88	163
ED2*-*t*[b]	-	-	-	-	-	-
ED3-*t*	-7.73	-10.5	2.75	0.0021	2.83	113
ED4-*t*	-6.33	-9.08	2.75	0.0008	2.42	166
B3LYP-D3:						
ED1-*t*[c]	-	-	-	-	-	-
ED2-*t*	-32.1	-37.1	5.03	0.0123	1.86	163
ED2*-*t*	-32.1	-37.1	5.02	0.0112	1.88	162
ED3-*t*	-17.0	-20.4	3.43	0.0018	2.89	104
ED4-*t*	-19.7	-23.4	3.76	-0.0014	2.45	134
ωB97X-D:						
ED1-*t*	-37.2	-42.9	5.76	0.0166	1.83	161
ED2-*t*[b]	-	-	-	-	-	-
ED2*-*t*	-30.3	-35.1	4.78	0.0124	1.88	162
ED3-*t*	-15.4	-18.5	3.07	0.0026	2.78	109
ED4-*t*	-17.2	-20.8	3.58	-0.0003	2.44	135
M06-2X:						
ED1-*t*[d]	-40.8	-46.0	5.15	0.0165	1.82	158
ED2-*t*[c]	-	-	-	-	-	-
ED2*-*t*	-32.0	-37.0	4.89	0.0112	1.89	156
ED3-*t*	-17.5	-20.6	3.01	0.0028	2.27	106
ED4-*t*	-21.0	-24.9	3.83	-0.0007	2.44	127
MP2:						
ED1-*t*	-41.6	-47.2	5.64	0.0179	1.80	116
ED2-*t*	-35.0	-39.8	4.82	0.0134	1.84	161
ED2*-*t*	-33.5	-38.1	4.61	0.0127	1.86	162
ED3-*t*	-19.4	-22.5	3.05	0.0029	2.70	109
ED4-*t*	-22.3	-25.5	3.14	-0.0008	2.43	130

a: Calculated with CCSD(T)-F12a/VDZ-F12, DFT/aug-cc-pVTZ and MP2/aug-cc-pVTZ methods.
b: Unable to optimize.
c: Terminated with an imaginary frequency with default optimization criteria.
d: Has an imaginary frequency: 32i cm^{-1}.

Table S12: Observed and calculated fundamental OH-stretching frequencies ($\tilde{\nu}$ in cm^{-1}), redshifts ($\Delta\tilde{\nu}$ in cm^{-1}) and intensities (f) for the EtOH monomer (*gauche*) and the EtOH·DMSO complex.

Observed			Calculated[a]			
Compound	$\tilde{\nu}_{\max}$	$\Delta\tilde{\nu}$[b]	Conformer[d]	$\tilde{\nu}$	$\Delta\tilde{\nu}$[b]	f
EtOH	3669[c]	-	EtOH	3639	-	2.58×10^{-6}
EtOH·DMSO	3429	240	ED1	3326	313	1.30×10^{-4}
	3505	164	ED2	3402	238	1.28×10^{-4}
			ED2*	3403		1.26×10^{-4}

a: Calculated with the 2D+2D LMPT model and the B3LYP/aug-cc-pVTZ method.[24] EtOH is in the *gauche* confirguration. The EtOH monomer frequency is calculated with a 2D local mode model.
b: $\Delta\tilde{\nu} = \tilde{\nu}_{\text{Alcohol}}$ - $\tilde{\nu}_{\text{complex}}$.
c: Determined as the Q-branch, we use a weighted band center of the two conformers.
d: The conformer abbreviations are defined in Figures S29 and S30.

Table S13: Calculated frequencies ($\tilde{\nu}$ in cm^{-1}) and intensities (f) with LMPT model and the B3LYP/aug-cc-pVTZ method. The EtOH monomer (*trans*) frequency is calculated with a 2D local mode model.

	EtOH	ED1	ED2	ED2* [a]
$\tilde{\nu}$	3655	3310	3407	3422
f	2.93×10^{-6}	1.39×10^{-4}	1.41×10^{-4}	1.28×10^{-4}

a: Calculated with the MP2/aug-cc-pVTZ method, with this method the corresponding EtOH monomer values are 3678 and 5.90×10^{-6}.

S2.5 NCI calculations of the MeOH complexes

In the 2D NCI plot, the reduced density gradient, $s = \frac{|\nabla\rho|}{2(3\pi^2)^{1/3}\rho^{4/3}}$, is plotted against the product of the sign of the second eigenvalue of the Hessian and the electron density, $\text{sign}(\lambda_2)\rho$. Troughs indicate the presence of non-covalent interactions. Troughs with $\text{sign}(\lambda_2)\rho < 0$ and $\text{sign}(\lambda_2)\rho > 0$ represent attractive and repulsive interactions, respectively. The strength of an interaction depends on the magnitude of ρ. The color code is applied to differentiate between attractive interactions (blue), very weak non-covalent interactions (green) and repulsive interactions (red). The color code also applies to the 3D NCI isosurfaces that visualize the $\text{sign}(\lambda_2)\rho$,s points in 3D space of the molecule.

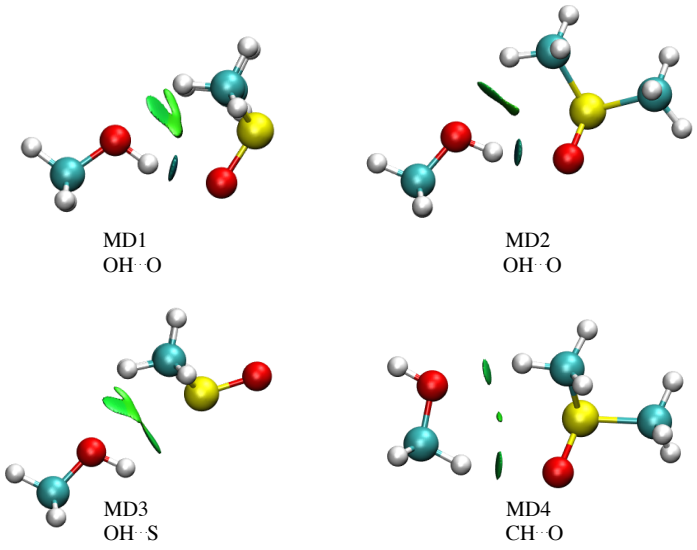

Figure S32: CCSD(T)-F12a/VDZ-F12 3D NCI isosurfaces, which visualize the ($\text{sign}(\lambda_2)\rho$,s) points in 3D space of the molecule with a s value of 0.5 a.u..

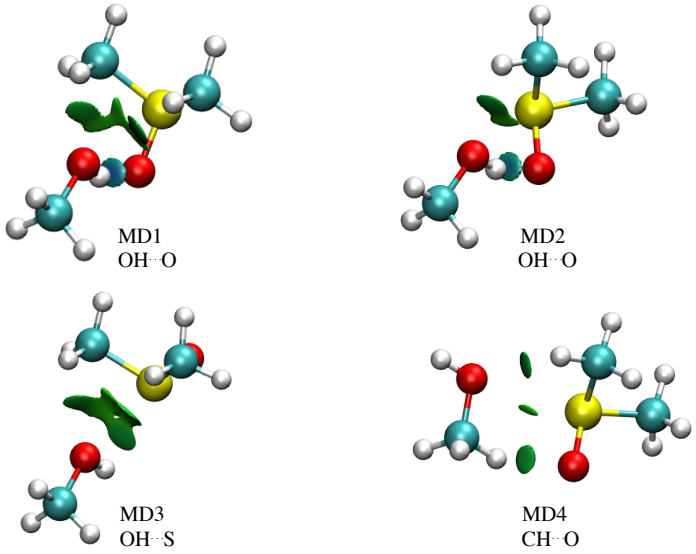

Figure S33: The 3D NCI isosurfaces shown in Figure S32 where the molecules are orientated differently.

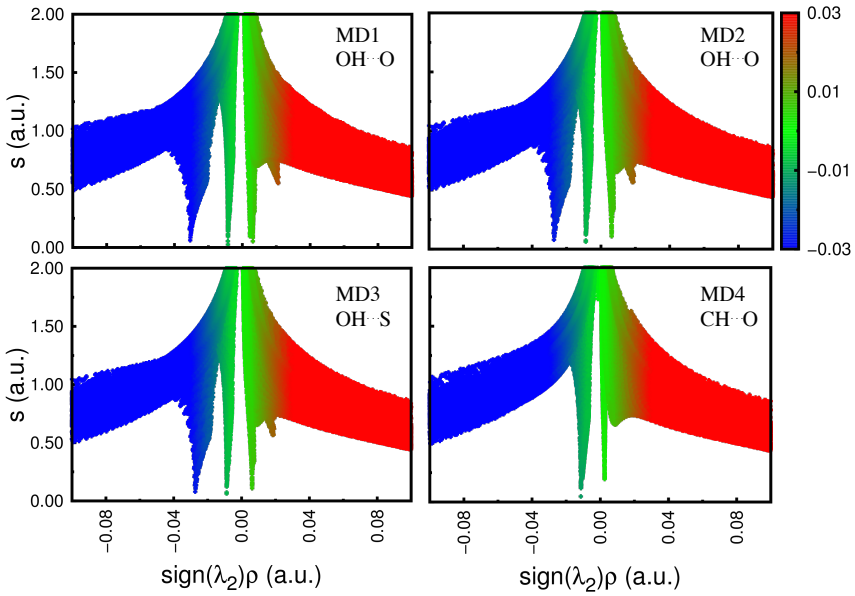

Figure S34: CCSD(T)-F12a/VDZ-F12 2D NCI plot of the reduced density gradient, s, versus the product of the sign of the second eigenvalue of the Hessian and the electron density, $\text{sign}(\lambda_2)\rho$. Troughs indicate the presence of non-covalent interactions. Troughs with $\text{sign}(\lambda_2)\rho < 0$ and $\text{sign}(\lambda_2)\rho > 0$ represent attractive and repulsive interactions, respectively. The strength of an interaction depends on the magnitude of ρ. In the 2D NCI plots and 3D NCI isosurfaces, a three color code is applied to differentiate between attractive interactions (blue), very weak non-covalent interactions (green) and repulsive interactions (red).

S2.6 Normal mode frequencies and intensities

MeOH·DMSO:

Table S14: Normal mode calculated B3LYP/aug-cc-pVTZ frequencies ($\tilde{\nu}$ in cm^{-1}) of all 3N-6 vibrations in MeOH, DMSO and the MeOH·DMSO conformers (Figures 1 and S26). The values in bold correspond to the SO-stretching vibration.

MeOH	DMSO	MD1	MD2	MD3	MD4
291	181	28	20	27	27
1039	222	54	32	29	41
1076	279	71	59	42	61
1171	314	112	103	70	86
1366	365	125	115	90	100
1477	627	196	175	93	109
1498	657	208	187	189	193
1509	892	236	225	230	242
2994	929	283	281	279	284
3040	954	318	343	315	308
3108	1024	386	365	366	321
3829	**1080**	635	635	379	366
-	1312	665	656	632	631
-	1333	713	673	663	662
-	1442	908	903	898	901
-	1455	946	939	938	933
-	1459	960	960	963	960
-	1476	1038	1033	1027	1022
-	3037	**1050**	**1049**	1039	1033
-	3040	1064	1065	1078	**1070**
-	3131	1137	1129	**1087**	1079
-	3135	1173	1173	1172	1174
-	3143	1321	1320	1312	1316
-	3143	1342	1343	1332	1340
-	-	1445	1439	1365	1365
-	-	1448	1444	1446	1443
-	-	1463	1456	1459	1456
-	-	1464	1460	1460	1463

Table continued on next page.

MeOH	DMSO	MD1	MD2	MD3	MD4
-	-	1477	1476	1476	1484
-	-	1481	1478	1478	1487
-	-	1497	1496	1498	1510
-	-	1514	1512	1510	1511
-	-	2984	2982	3001	2998
-	-	3025	3022	3041	3031
-	-	3038	3039	3042	3038
-	-	3041	3042	3049	3047
-	-	3087	3086	3110	3123
-	-	3134	3134	3138	3127
-	-	3138	3137	3140	3133
-	-	3144	3145	3144	3139
-	-	3145	3146	3146	3142
-	-	3511	3587	3788	3830

Table S15: Calculated B3LYP/aug-cc-pVTZ intensities (f) of all 3N-6 vibrations in MeOH, DMSO and the MeOH·DMSO conformers (Figures 1 and S26). The values in bold correspond to the SO-stretching vibration.

MeOH	DMSO	MD1	MD2	MD3	MD4
1.98×10^{-5}	1.88×10^{-11}	1.35×10^{-6}	9.90×10^{-7}	6.43×10^{-7}	9.93×10^{-7}
2.27×10^{-5}	5.54×10^{-8}	1.09×10^{-7}	9.78×10^{-7}	3.54×10^{-6}	1.15×10^{-6}
2.81×10^{-7}	6.03×10^{-8}	3.89×10^{-6}	2.81×10^{-6}	1.27×10^{-6}	1.03×10^{-6}
8.05×10^{-8}	1.54×10^{-6}	4.00×10^{-8}	4.23×10^{-7}	5.16×10^{-8}	4.97×10^{-7}
4.60×10^{-6}	1.26×10^{-6}	1.80×10^{-6}	4.26×10^{-7}	6.71×10^{-7}	3.50×10^{-6}
5.92×10^{-7}	1.62×10^{-6}	1.73×10^{-8}	7.56×10^{-8}	1.34×10^{-7}	2.51×10^{-6}
5.58×10^{-7}	3.00×10^{-6}	8.61×10^{-7}	4.30×10^{-8}	3.51×10^{-9}	7.56×10^{-9}
1.01×10^{-6}	3.34×10^{-7}	1.79×10^{-7}	1.17×10^{-7}	3.78×10^{-8}	9.12×10^{-8}
1.18×10^{-5}	1.29×10^{-6}	3.53×10^{-7}	1.63×10^{-7}	8.59×10^{-8}	3.80×10^{-7}
9.99×10^{-6}	2.06×10^{-6}	1.03×10^{-6}	3.77×10^{-6}	1.47×10^{-6}	1.71×10^{-5}
4.57×10^{-6}	2.96×10^{-6}	2.12×10^{-6}	1.13×10^{-6}	1.18×10^{-6}	2.03×10^{-6}
5.82×10^{-6}	$\mathbf{2.56}\times10^{-5}$	9.74×10^{-7}	1.39×10^{-6}	1.33×10^{-5}	1.44×10^{-6}
-	1.54×10^{-7}	1.36×10^{-6}	1.30×10^{-5}	1.27×10^{-6}	1.46×10^{-6}
-	1.47×10^{-6}	1.33×10^{-5}	4.03×10^{-6}	2.75×10^{-6}	2.95×10^{-6}
-	1.62×10^{-6}	6.58×10^{-7}	4.60×10^{-7}	2.45×10^{-7}	4.19×10^{-7}
-	8.53×10^{-7}	1.12×10^{-6}	1.73×10^{-6}	1.35×10^{-6}	1.57×10^{-6}
-	2.48×10^{-9}	3.73×10^{-6}	4.45×10^{-6}	1.99×10^{-6}	2.90×10^{-6}
-	3.16×10^{-6}	6.23×10^{-6}	3.08×10^{-6}	4.14×10^{-6}	1.23×10^{-5}
-	7.42×10^{-7}	$\mathbf{3.80}\times10^{-5}$	$\mathbf{4.22}\times10^{-5}$	3.69×10^{-5}	4.26×10^{-6}
-	1.47×10^{-6}	1.33×10^{-5}	1.33×10^{-5}	1.86×10^{-5}	$\mathbf{2.94}\times10^{-5}$
-	1.76×10^{-8}	3.74×10^{-6}	3.54×10^{-6}	$\mathbf{1.05}\times10^{-5}$	1.81×10^{-6}
-	1.90×10^{-6}	1.44×10^{-7}	1.33×10^{-7}	1.31×10^{-7}	1.37×10^{-7}
-	2.24×10^{-7}	1.42×10^{-7}	7.71×10^{-8}	2.43×10^{-7}	8.65×10^{-8}
-	5.95×10^{-7}	1.85×10^{-6}	2.00×10^{-6}	1.48×10^{-6}	1.43×10^{-6}
-	-	1.23×10^{-6}	1.01×10^{-5}	1.41×10^{-5}	4.49×10^{-6}
-	-	1.34×10^{-5}	9.31×10^{-6}	1.20×10^{-6}	1.32×10^{-6}
-	-	7.64×10^{-6}	1.64×10^{-6}	4.51×10^{-8}	6.97×10^{-7}
-	-	5.97×10^{-8}	2.48×10^{-7}	1.01×10^{-6}	2.47×10^{-7}

Table continued on next page.

MeOH	DMSO	MD1	MD2	MD3	MD4
-	-	1.82×10^{-7}	2.13×10^{-6}	8.07×10^{-7}	2.14×10^{-6}
-	-	4.47×10^{-6}	1.61×10^{-6}	3.20×10^{-6}	1.14×10^{-6}
-	-	4.80×10^{-7}	4.87×10^{-7}	6.51×10^{-7}	3.63×10^{-7}
-	-	8.69×10^{-7}	5.24×10^{-7}	1.13×10^{-6}	3.95×10^{-7}
-	-	1.92×10^{-5}	1.84×10^{-5}	1.39×10^{-5}	1.49×10^{-5}
-	-	1.08×10^{-5}	1.14×10^{-5}	8.29×10^{-7}	2.46×10^{-6}
-	-	6.59×10^{-7}	7.20×10^{-7}	1.02×10^{-6}	1.97×10^{-6}
-	-	2.24×10^{-6}	1.65×10^{-6}	8.23×10^{-6}	9.04×10^{-6}
-	-	7.93×10^{-6}	8.29×10^{-6}	4.33×10^{-6}	5.72×10^{-8}
-	-	6.97×10^{-8}	3.77×10^{-8}	3.07×10^{-8}	4.08×10^{-7}
-	-	5.80×10^{-7}	1.45×10^{-6}	1.11×10^{-6}	1.80×10^{-6}
-	-	1.66×10^{-7}	1.93×10^{-7}	2.67×10^{-7}	2.91×10^{-6}
-	-	3.19×10^{-7}	5.03×10^{-7}	2.22×10^{-7}	5.07×10^{-7}
-	-	1.22×10^{-4}	1.25×10^{-4}	1.41×10^{-5}	5.37×10^{-6}

MeOH·acetone:

Table S16: Normal mode calculated B3LYP/aug-cc-pVTZ frequencies ($\tilde{\nu}$ in cm^{-1}) and intensities (f) of all 3N-6 vibrations in acetone and the MeOH·acetone MA1 conformer (Figure 1).

$\tilde{\nu}$		f	
Acetone	MA1	Acetone	MA1
28	19	0	1.84×10^{-6}
132	34	1.53×10^{-8}	2.01×10^{-8}
381	51	3.26×10^{-7}	1.16×10^{-6}
491	54	1.07×10^{-7}	1.02×10^{-6}
535	104	2.68×10^{-6}	6.59×10^{-7}
783	109	3.57×10^{-7}	1.77×10^{-8}
887	129	0	2.49×10^{-8}
887	181	1.78×10^{-6}	5.02×10^{-8}
1085	390	1.63×10^{-9}	8.46×10^{-7}
1121	495	4.88×10^{-7}	8.74×10^{-9}
1234	551	1.35×10^{-5}	3.61×10^{-6}
1388	641	3.55×10^{-6}	1.46×10^{-5}
1388	792	1.02×10^{-5}	2.03×10^{-7}
1460	891	9.72×10^{-8}	3.07×10^{-8}
1466	901	0	1.31×10^{-6}
1470	1062	5.75×10^{-6}	2.30×10^{-5}
1488	1092	3.54×10^{-6}	6.34×10^{-8}
1782	1124	3.66×10^{-5}	3.38×10^{-6}
3025	1125	1.70×10^{-7}	1.75×10^{-6}
3033	1172	1.38×10^{-6}	1.23×10^{-7}
3077	1248	0	1.32×10^{-5}

Table continued on next page.

$\tilde{\nu}$		f	
Acetone	MA1	Acetone	MA1
3084	1391	3.19×10^{-6}	7.92×10^{-6}
3138	1396	2.23×10^{-6}	9.13×10^{-6}
3139	1432	1.19×10^{-6}	1.24×10^{-5}
-	1462	-	5.03×10^{-7}
-	1465	-	1.38×10^{-6}
-	1475	-	5.96×10^{-6}
-	1477	-	2.77×10^{-6}
-	1490	-	3.56×10^{-6}
-	1497	-	3.87×10^{-7}
-	1512	-	5.65×10^{-7}
-	1762	-	4.69×10^{-5}
-	2981	-	1.73×10^{-5}
-	3021	-	1.17×10^{-5}
-	3027	-	1.82×10^{-7}
-	3034	-	1.49×10^{-6}
-	3078	-	2.19×10^{-7}
-	3086	-	2.14×10^{-6}
-	3089	-	7.95×10^{-6}
-	3141	-	1.49×10^{-6}
-	3143	-	3.67×10^{-8}
-	3638	-	1.17×10^{-4}

References

(1) Perchard, J. P. Anharmonicity and hydrogen bonding. III. Analysis of the near infrared spectrum of water trapped in argon matrix. *Chem. Phys.* **2001**, *273*, 217–233.

(2) Barnes, A. J.; Hallam, H. E. Infra-red cryogenic studies. Part 4.-Isotopically substituted methanols in argon matrices. *Trans. Faraday Soc.* **1970**, *66*, 1920–1931.

(3) Perchard, J. P.; Mielke, Z. Anharmonicity and hydrogen bonding: I. A near-infrared study of methanol trapped in nitrogen and argon matrices. *Chem. Phys.* **2001**, *264*, 221–234.

(4) Doroshenko, I.; Pogorelov, V.; Sablinskas, V.; Balevicius, V. Matrix-isolation study of cluster formation in methanol: O-H stretching region. *J. Mol. Liq.* **2010**, *157*, 142–145.

(5) Tevault, D. E.; Mowery, R. L.; Smardzewski, R. R. Ozone and oxygen atom reactions with dimethylsulfide and methanethiol in argon matrices. *J. Chem. Phys.* **1981**, *74*, 4480–4487.

(6) Provencal, R. A.; Paul, J. B.; Roth, K.; Chapo, C.; Casaes, R. N.; Saykally, R. J.; Tschumper, G. S.; Schaefer, H. F. Infrared cavity ringdown spectroscopy of methanol clusters: Single donor hydrogen bonding. *J. Chem. Phys.* **1999**, *110*, 4258–4267.

(7) Häber, T.; Schmitt, U.; A. Suhm, M. FTIR-spectroscopy of molecular clusters in pulsed supersonic slit-jet expansions. *Phys. Chem. Chem. Phys.* **1999**, *1*, 5573–5582.

(8) Wugt Larsen, R.; Zielke, P.; Suhm, M. A. Hydrogen-bonded OH stretching modes of methanol clusters: A combined IR and Raman isotopomer study. *J. Chem. Phys.* **2007**, *126*, 194307.

(9) Zielke, P.; Suhm, M. A. Concerted proton motion in hydrogen-bonded trimers: A spontaneous Raman scattering perspective. *Phys. Chem. Chem. Phys.* **2006**, *8*, 2826–2830.

(10) Zhang, X. K.; Lewars, E. G.; March, R. E.; Parnis, J. M. Vibrational spectrum of the acetone-water complex: A matrix isolation FTIR and theoretical study. *J. Phys. Chem.* **1993**, *97*, 4320–4325.

(11) Han, S. W.; Kim, K. Infrared matrix isolation study of acetone and methanol in solid argon. *J. Phys. Chem.* **1996**, *100*, 17124–17132.

(12) Hansen, A. S.; Du, L.; Kjaergaard, H. G. Positively charged phosphorus as a hydrogen bond acceptor. *J. Phys. Chem. Lett.* **2014**, *5*, 4225–4231.

(13) Fawcett, W. R.; Kloss, A. A. Solvent-induced frequency shifts in the infrared spectrum of dimethyl sulfoxide in organic solvents. *J. Phys. Chem.* **1996**, *100*, 2019–2024.

(14) Shun-Li, O.; Nan-Nan, W.; Jing-Yao, L.; Cheng-Lin, S.; Zuo-Wei, L.; Shu-Qin, G. Investigation of hydrogen bonding in neat dimethyl sulfoxide and binary mixture (dimethyl sulfoxide + water) by concentration-dependent Raman study and *ab initio* calculation. *Chinese Phys. B* **2010**, *19*, 123101.

(15) Niazazari, N.; Zatikyan, A. L.; Markarian, S. A. *Ab initio* and DFT study of hydrogen bond interactions between ascorbic acid and dimethylsulfoxide based on FT-IR and FT-Raman spectra. *Spectrochim. Acta A* **2013**, *110*, 217–225.

(16) Du, L.; Lane, J. R.; Kjaergaard, H. G. Identification of the dimethylamine-trimethylamine complex in the gas phase. *J. Chem. Phys.* **2012**, *136*, 184305.

(17) Chung, S.; Hippler, M. Infrared spectroscopy of hydrogen-bonded $CHCl_3$-SO_2 in the gas phase. *J. Chem. Phys.* **2006**, *124*, 214316.

(18) Hippler, M. Quantum chemical study and infrared spectroscopy of hydrogen-bonded $CHCl_3$-NH_3 in the gas phase. *J. Chem. Phys.* **2007**, *127*, 084306.

(19) Du, L.; Mackeprang, K.; Kjaergaard, H. G. Fundamental and overtone vibrational spectroscopy, enthalpy of hydrogen bond formation and equilibrium constant determi-

nation of the methanol-dimethylamine complex. *Phys. Chem. Chem. Phys.* **2013**, *15*, 10194–10206.

(20) Hansen, A. S.; Du, L.; Kjaergaard, H. G. The effect of fluorine substitution in alcohol-amine complexes. *Phys. Chem. Chem. Phys.* **2014**, *16*, 22882–22891.

(21) Andersen, C. L.; Jensen, C. S.; Mackeprang, K.; Du, L.; Jørgensen, S.; Kjaergaard, H. G. Similar strength of the NH$\cdots$O and NH$\cdots$S hydrogen bonds in binary complexes. *J. Phys. Chem. A* **2014**, *118*, 11074–11082.

(22) Reece, I. H.; Werner, R. L. Intermolecular interaction in solution-II The association of alcohols in solution and in the vapour phase. *Spectrochim. Acta A* **1968**, *24*, 1271–1282.

(23) Kollipost, F.; Domanskaya, A. V.; Suhm, M. A. Microscopic roots of alcohol-ketone demixing: Infrared spectroscopy of methanol-acetone clusters. *J. Phys. Chem. A* **2015**, *119*, 2225–2232.

(24) Mackeprang, K.; Kjaergaard, H. G. Vibrational transitions in hydrogen bonded bimolecular complexes - a local mode perturbation theory approach to transition frequencies and intensities. *J. Mol. Spectrosc.* **2017**, *334*, 1–9.

(25) Mackeprang, K.; Kjaergaard, H. G.; Salmi, T.; Hänninen, V.; Halonen, L. The effect of large amplitude motions on the transition frequency redshift in hydrogen bonded complexes: A physical picture. *J. Chem. Phys.* **2014**, *140*, 184309.

(26) Mackeprang, K.; Hänninen, V.; Halonen, L.; Kjaergaard, H. G. The effect of large amplitude motions on the vibrational intensities in hydrogen bonded complexes. *J. Chem. Phys.* **2015**, *142*, 094304.

(27) Dhumal, N. R. Electronic structure, molecular electrostatic potential and hydrogen bonding in DMSO-X complexes (X = ethanol, methanol and water). *Spectrochim. Acta A* **2011**, *79*, 654–660.

(28) Biswal, H. S.; Wategaonkar, S. Sulfur, not too far behind O, N, and C: SH$\cdots\pi$ hydrogen bond. *J. Phys. Chem. A* **2009**, *113*, 12774–12782.

(29) Howard, D. L.; Kjaergaard, H. G. Hydrogen bonding to divalent sulfur. *Phys. Chem. Chem. Phys.* **2008**, *10*, 4113–4118.

(30) Arunan, E.; Desiraju, G. R.; Klein, R. A.; Sadlej, J.; Scheiner, S.; Alkorta, I.; Clary, D. C.; Crabtree, R. H.; Dannenberg, J. J.; Hobza, P. et al. Definition of the hydrogen bond (IUPAC Recommendations 2011). *Pure Appl. Chem.* **2011**, *83*, 1637–1641.